Australian Government
Department of Defence
Defence Science and
Technology Organisation

# Distribution of X-Band High Resolution and High Grazing Angle Sea Clutter

*Yunhan Dong*

**Electronic Warfare and Radar Division**
**Defence Science and Technology Organisation**

DSTO-RR-0316

## ABSTRACT

This report studies the spatial distribution of X-band, high resolution and high grazing angle polarimetric sea clutter data. The K distribution usually provides a good fit for the distribution of the VV polarised data. The HH polarised data is spikiest and its distribution exhibits a sudden departure from the K distribution in the tail region, which usually requires the KA or the similar distributions to achieve a better fit in the tail region. Due to drawbacks of the KA distribution, this report proposes the KK and WW distribution models to fit the distribution of sea clutter with spikes. It is found that the KK distribution provides overall the best fit. Distributions of the sum of K and Weibull distributed samples are also presented.

*Published by*

*Defence Science and Technology Organisation*
*PO Box 1500*
*Edinburgh South Australia 5111*

*Telephone: (08) 8259 5555*
*Fax: (08) 8259 6567*


*AR-013-708*
*July 2006*

**APPROVED FOR PUBLIC RELEASE**

# Distribution of X-Band High Resolution and High Grazing Angle Sea Clutter

## EXECUTIVE SUMMARY

This report contributes to the delivery of *Milestone 4.1.1.1.1: High grazing angle sea clutter and target signatures* in the AIR 7000 S&T Plan (Annex C – Technical Support Plan). The outcomes of the analysis contained herein will also form a component of the model delivered for *Milestone 4.1.1.1.2: Radar modelling capability development – maritime* of the Technical Support Plan. These activities are aimed at better understanding the radar performance drivers for operation of High Altitude Long Endurance (HALE) unmanned aerial vehicles (UAVs) in the maritime surveillance role, and therefore reducing risk in any acquisition decision.

Sea clutter distributions have been studied for many decades. However most of these studies are based on sea clutter data collected at low grazing angles and for applications of radar mounted on ships or at the coast. Very little analysis of high grazing angle sea clutter has been published in the open literature. The next generation of airborne maritime radar surveillance systems, such as high altitude UAVs, views the sea surface at much higher grazing angles. Sea clutter returns at low grazing angles are often dominated by multipath, shadowing and ducting mechanisms, whereas the Bragg scattering from rough surfaces and scattering from whitecaps often dominate at high grazing angles. These different scattering mechanisms mean that the nature and characteristics of sea clutter at high and low grazing angles are different. In addition, the resolution of the future radar tends to be higher. The finer the radar resolution, the more discrete sea spikes in sea clutter. Understanding and modelling of such spikes are important for the prediction of radar performance and for guidance in developing improved target detection algorithms. Therefore searching for distribution models which provide precise distribution agreement especially in the tail region is necessary in sea clutter distribution studies in order to improve radar performance.

In support of Project AIR 7000, DSTO conducted a sea clutter collection trial in the Southern Ocean approximately 100 km south of Port Lincoln in South Australia in 2004 using the DSTO developed X-band, fully polarised airborne radar imaging system,

Ingara. Data were collected with incidence angle varying from approximate $45^o$ to $80^o$, on 8 separate days over an 18-day period. The wind and wave conditions were also recorded using a wave buoy deployed nearby and the information provided by the Royal Australian Navy's Directorate of Oceanography and Meteorology, and the Australian Government Bureau of Meteorology.

The data used in this report are real aperture high range resolution (0.75 m) data with the radar operated in a circular spotlight mode. The radar could therefore be considered to look at the same spot but with different incidence and azimuth angles. Each dataset used in the analysis consists of approximately $10^6$ samples, corresponding to a span of $3.5^o$ to $8^o$ in incidence angle change, depending on nominal incidence angle, and a span of $5^o$ in azimuth angle change. Since the nominal incidence angle is in the plateau region and the span of the azimuth angle is narrow, we can consider the data distribution to be as the spatial distribution. The size of the samples in each dataset provides a reliable data distribution up to 1-cdf equal to the $10^{-5}$ level.

It is found that the mean clutter varies periodically in azimuth with the maxima and the minima in the upwind and crosswind directions, respectively, and the second peak in the downwind direction. The shape parameter of clutter distributions, however, does not show a noticeable azimuthal pattern correlating to wave/wind directions.

The VV polarised data is with the lowest spiky level compared to the HH and HV data. In general the VV data can be fitted by a K distribution with the shape parameter varying from about 4 to 25.

The HH polarised data is spikiest and its distribution exhibits a sudden departure from the K distribution in the tail region, often in the region of 1-cdf (cumulative distribution function) equal to $10^{-3}$ and beyond. The phenomenon of the sudden departure is believed to be attributed by sea discrete spikes. The finer the radar resolution, the severer is the phenomenon. This observation indicates that the traditional K distribution might not be precise enough to model the distribution of sea clutter with spikes.

The KA distribution, which has been more recently proposed in the literature to model the distribution of sea clutter with spikes, has significantly improved the agreement between the data and model distributions in the tail region. However, the KA distribution cannot be expressed in closed form, so it is computationally very expensive. It also imposes a difficulty for the analysis of radar performance, as the analysis often involves the clutter distribution function. Aimed at simplifying the distribution function, this report proposes a KK distribution, which is a mixture of two K distributions of which one representing the distribution of Bragg/whitecap scatterers and the other for the distribution of sea spikes. It shows that the KK

distribution is as good as the KA distribution in terms of agreement in the tail region. In addition, the KK distribution introduces the least distortion to the K distribution in the low and mid regions. Mathematically, a KK distribution is simply a sum of two K distributions.

Since the Weibull distribution is very close to the K distribution, this report also proposes a WW distribution to improve the agreement between the data pdf and the modelled pdf in the tail region. A WW distribution is a mixture of two Weibull distributions. In general, a Weibull distribution converges a little faster than a K distribution for shape parameters normally found in sea clutter statistics, which often leads to a bigger discrepancy between the data pdf and the Weibull pdf in the tail region. The Weibull fit, even for the VV data is not as good as the K fit. This however can be compensated if a WW distribution is used, as the convergence of the WW distribution is tuneable. The results show that the fitness of the WW distribution in the tail region is comparable to the KK or KA distribution. However, in the low and mid region, the agreement between the data pdf and the WW pdf is not as good as that between the data pdf and the KK (or K) pdf.

The use of the KA, KK and WW distributions improves the agreement between the data and fitted distributions in the tail region. It is shown that the difference between the data cdf and the K cdf for the HH polarised data at the 1-cdf equal to $10^{-5}$ level can be as big as about −7dB, but the difference can be reduced to about ±1dB if the KK distribution is used to model the data distribution. Since the KK distribution provides the least distortions to the K distribution in the low and mid regions, the fit improvement in the tail region does not worsen the agreement in the low and mid region.

The report also proves that a Weibull distribution can be transformed to a Rayleigh or gamma distribution and vice versa through a non-linear but simple mapping. Therefore, in the case where clutter data is modelled as a Weibull distribution, the data may be first transformed accordingly and then treated as a Rayleigh or gamma distribution, as the Rayleigh or gamma distribution is much easier to be dealt with. For simulation, a Weibull distributed dataset can be easily generated from a transform of a Rayleigh distributed dataset.

CFAR schemes often employ local statistics of clutter to adaptively set the threshold for target detection. This report also discusses the distribution of the sum of K or Weibull distributed samples. A formula in closed form approaches the distribution of the sum of Weibull distributed samples, which does not have close form, has been proposed. Its correctness has been numerically verified using both the convolution method and simulated data. No noticeable error between the values given by the formula and the values numerically computed from the convolution method or simulated data has been found.

# Author

*Yunhan Dong*
Electronic Warfare Division

*Dr Yunhan Dong received his Bachelor and Master degrees in 1980s in China and PhD in 1995 at UNSW, Australia, all in electrical engineering. He then worked at UNSW from 1995 to 2000, and Optus Telecommunications Inc from 2000 to 2002. He joined DSTO as a Senior Research Scientist in 2002. His research interests are primarily in radar signal and image processing and clutter analysis. Dr Dong was a recipient of both the Postdoctoral Research Fellowships and Research Fellowships from the Australian Research Council.*

# Contents

# 1. Introduction

Sea clutter distributions have been studied for many decades. However most of these studies are based on sea clutter data collected at low grazing angles and for applications of radar mounted on ships or at the coast. The next generation of airborne maritime radar surveillance systems, such as high altitude unmanned aerial vehicles (UAVs), views the sea surface at much higher grazing angles. Sea clutter returns at low grazing angles are often dominated by multipath, shadowing and ducting mechanisms, whereas the Bragg scattering from rough surfaces and scattering from whitecaps often dominate at high grazing angles (Long, 2001). These different scattering mechanisms indicate that the nature and characteristics of sea clutter at high and low grazing angles should be different. Very little analysis of high angle sea clutter has been published in the open literature.

In support of Project AIR 7000, DSTO conducted a sea clutter collection trial in the Southern Ocean approximately 100 km south of Port Lincoln in South Australia in 2004 using the DSTO developed X-band, fully polarised airborne radar system, Ingara (Crisp et al, 2006). Data were collected with incidence angle varying from approximate $45^o$ to $80^o$, on 8 separate days over an 18-day period. The data used in this report was real aperture high range resolution (0.75 m) data with the radar operated in a circular spotlight mode. The radar can therefore be considered to look at the same spot but with different azimuth and elevation angles. The wind and wave conditions were also recorded using a wave buoy deployed nearby and additional information was provided by the Royal Australian Navy's Directorate of Oceanography and Meteorology, and the Australian Government Bureau of Meteorology.

This report concentrates on clutter distribution studies. Other topics such as correlation, optimal polarisation for discriminating small targets from clutter etc will be reported in the future. In this report we pay less attention to the physical modelling but focus on the distribution studies. The K and Weibull distributions are widely used to fit sea clutter distribution (Jao, 1984, Watts, 1985, 1987, Ward et al, 1990, Oliver, 1993, Antipov, 1998, Billingsley, 2002) and the lognormal distribution is also reported in some cases (Long, 2001). More recently, the KA distribution has been suggested to improve the fit in the tail region, usually in the region of 1-cdf (cumulative distribution function) equal to $10^{-3}$ and beyond (Ward and Tough, 2002, Watts and Tough, 2005). It is important to have the fit in the tail region as precise as possible, so that the constant false alarm rate (CFAR) based detection algorithms and radar performance analysis can be processed accurately.

We first review the K and Weibull distributions in Sections 2 and 3, respectively. Data with known distributions and parameters are generated, and the accuracy of

parameter estimation schemes is quantitatively assessed. We derive in Section 3 that a Weibull distribution can be transformed to a Rayleigh or gamma distribution and vice versa. One immediate application of this derivation is that a Weibull distributed dataset can be generated simply from a Rayleigh distributed dataset. In radar applications, if clutter is Weibull distributed, the data can be transformed into the Rayleigh or gamma distributed for further processing.

CFAR processing schemes set the detection threshold adaptively based on the local statistics of clutter. An example of such a scheme is the cell averaging (CA) CFAR which set the threshold adaptively by estimating the sum /mean level in a window of N range samples surrounding the cell under test (CUT). We need therefore to study the distribution of the sum / mean of N K or Weibull distributed samples. Subsection 2.2 discusses the distribution of the sum of N K-distributed samples. A formula in closed form approximating the sum of N Weibull distributed samples is proposed in Subsection 3.3.

Section 4 investigates the distribution of the sea clutter collected by DSTO. The co-polarised HH and VV as well as the cross-polarised HV data are studied. Discrepancies between the data and the fitted K and Weibull distributions indicate that the traditional K or Weibull distribution generally provides a conservative estimation in the tail region. This also drives us to search for better distribution models.

Section 5 discusses the KA distribution, which, by adding a component of sea spikes modelled as a discrete Poisson distribution, significantly improves the fit in the tail region. Since it cannot be expressed in closed form, the KA distribution is computationally expensive, and imposes a difficulty in the derivation of CFAR algorithms and radar performance analysis. A KK distribution (a mixture of two K-distributions) and a WW distribution (a mixture of two Weibull distributions) are proposed in Sections 6 and 7, respectively, to tackle the spike problem as the KA distribution does. Both the KK and WW distributions have the similar capability as the KA distribution to deal with the spike problem. Mathematically, however, the proposed KK and WW distributions are much simpler.

Finally Section 8 concludes the report.

# 2. K Distribution

Many studies have shown that sea clutter obeys a K distribution (Jao, 1984, Watts, 1985, 1987, Ward et al, 1990, Antipov, 1998, Oliver, 1993, Billingsley, 2002, Long, 2001). The K distribution has a phenomenological interpretation that clutter returns consist of a fast varying component modulated by a slow varying component. The slow varying component, also referred to as the varying local mean level, is root gamma distributed, and the fast varying component, referred to as speckle, is Rayleigh distributed (Watts,

1985, Ward et al, 1990, Watts, 1999). The primary difference between these two components lies in their temporal correlation properties. The speckle is largely decorrelated by radar frequency agility while the modulating component is not. Thus a radar system with pulse to pulse frequency agility will measure approximately unchanged value for the slow component over a beam dwell time (Ward and Tough, 2002).

For clutter modelling, some authors prefer using amplitude (linear detection), while the others use intensity (square law detection). This report adopts the amplitude distribution. In general, the distribution transform from one domain to the other can be readily done by,

$$p(v) = p(u)\left|du/dv\right| \tag{1}$$

once the relation $u = u(v)$ ($u(v)$ is monotonic), derivative $du/dv$ and the probability density function (pdf) $p(u)$ are known.

According to the expression for the compound K distribution (Watts, 1985, 1999), the pdf of the slow varying component, which is root gamma distributed, is given by,

$$p(y) = \frac{2b}{\Gamma(\nu)}(by)^{2\nu-1}\exp(-b^2y^2) \tag{2}$$

where $\nu$ is a shape parameter, $b$ is an intermediate scale parameter whose expression is given shortly, and $\Gamma(\cdot)$ is the gamma function.

The fast varying component, which is Rayleigh distributed, is,

$$p(x\,|\,y) = \frac{\pi x}{2y^2}\exp(-\frac{\pi x^2}{4y^2}) \tag{3}$$

The K-distributed function is the integral of (3) with respect to $y$, as,

$$p(x) = \int_0^\infty p(x\,|\,y)\,p(y)dy = \frac{2c}{\Gamma(\nu)}\left(\frac{cx}{2}\right)^{\nu} K_{\nu-1}(cx) \tag{4}$$

where $K_{\nu-1}(\cdot)$ is a modified Bessel function of the second kind of order $\nu-1$ and $c$ is a scale parameter whose expression is,

$$c = \frac{\sqrt{\pi}}{\bar{x}\,\Gamma(\nu)}\Gamma(\nu+1/2) \tag{5}$$

The relationship between $b$ and $c$ is $c = 2b\sqrt{\pi/4}$ and $\bar{x} = E\{x\}$ is the mean value of $x$.

$$\bar{x} = \frac{\sqrt{\pi}}{c\Gamma(\nu)}\Gamma(\nu + 1/2) \tag{6}$$

The second moment of $x$ is,

$$\overline{x^2} = \frac{4}{c^2\Gamma(\nu)}\Gamma(\nu+1) = \frac{4\nu}{c^2} \tag{7}$$

We often plot the clutter pdf on a log scale. To do so, let $z = 20\log_{10} x$, using the transform (1), we can write the K distribution of (4) on the dB scale as,

$$p(z) = k_0 \frac{2c}{\Gamma(\nu)} 10^{z/20}\left(\frac{c}{2}10^{z/20}\right)^{\nu} K_{\nu-1}(c10^{z/20}) \tag{8}$$

where $k_0 = \ln 10/20$ and $\ln(\cdot)$ is the natural logarithmic function. The first moment of $z$ is found to be (Dong, 2004),

$$\bar{z} = \frac{1}{2k_0}[2\ln 2 + \psi^{(0)}(1) - 2\ln c + \psi^{(0)}(\nu)] \tag{9}$$

where $\psi^{(n)}(x)$ is the Polygamma function, defined as the $(n+1)$th derivative of the logarithm of the Gamma function, $\frac{d^{n+1}}{dx^{n+1}}\left(\ln\Gamma(x)\right)$. Table 1 summarised the main properties of the K distribution.

*Table 1: Properties of the K distribution in linear and log domains.*

| Property | Linear domain | Log domain |
|---|---|---|
| Pdf | $p(x) = \frac{2c}{\Gamma(\nu)}\left(\frac{cx}{2}\right)^{\nu} K_{\nu-1}(cx)$ | $p(z) = k_0\frac{2c}{\Gamma(\nu)}10^{z/20}\left(\frac{c}{2}10^{z/20}\right)^{\nu} K_{\nu-1}(c10^{z/20})$ |
| Cdf | $P(x<t) = 1 - \frac{2}{\Gamma(\nu)}(ct/2)^{\nu}K_{\nu}(ct)$ | $P(z<t) = 1 - \frac{2}{\Gamma(\nu)}(c10^{t/20}/2)^{\nu}K_{\nu}(c10^{t/20})$ |
| First moment | $\bar{x} = \frac{\sqrt{\pi}}{c\Gamma(\nu)}\Gamma(\nu+1/2)$ | $\bar{z} = \frac{1}{2k_0}[2\ln 2 + \psi^{(0)}(1) - 2\ln c + \psi^{(0)}(\nu)]$ |
| Second moment | $\overline{x^2} = 4\nu/c^2$ | |

## 2.1 Parameter Estimation

The K distribution given by (4) has two parameters: scale factor $c$ and shape parameter $\nu$ which are normally unknown for arbitrary sea clutter data, even if the data is assumed to be K-distributed, and have to be estimated. There are various estimation schemes, and perhaps the most popular method is the maximum likelihood (ML) method which provides optimal parameter estimates in the sense that these estimates are the most probable parameters for the given data and pdf if there is no prior knowledge (Oliver, 1993 Antipov, 1998). For the K distribution, however, we cannot express the ML parameter estimates in closed form since the derivative of Bessel function $K_{\nu-1}(\cdot)$ does not exist in closed form. Using the Mellin transform, Oliver (1993) has derived an asymptotic expression for the K distribution, in which the K distribution is expressed as a gamma distribution with a modified factor. The corresponding approximate ML estimates for the asymptotic expression have then been derived. However, the resultant ML estimates are only applicable to the limit of a large number of looks in multi-look processed data such as synthetic aperture radar (SAR) data. Dong (2004) has proposed an algorithm searching the optimal parameters that maximise the log-likelihood function (eg, the log-marginal pdf). It is in an iterative algorithm, but does not require the derivatives of the Bessel function. We have found however, the proposed searching algorithm does not always work for K-distributed data in practice. The method is based on the product of the marginal pdfs of all data samples. If there exist some samples whose values are extremely small or large, then the pdf of these samples would be approaching zero. If the numerical precision of the Bessel function is limited (e.g. as in the standard MATLAB library) then the numerical value of these marginal pdfs becomes zero (minus infinity in the log domain) and the method fails.

Apart from the ML method, there are a number of moment-based methods which have been reviewed by Redding (1999). The algorithm using the first moment in the linear domain, $\overline{x} \approx \hat{x} = \frac{1}{N}\sum_{i=1}^{N} x_i$ and the first moment in the log domain, $\overline{z} \approx \hat{z} = \frac{1}{N}\sum_{i=1}^{N} z_i$ together to estimate the scale and shape parameters usually provides a very close result to the ML estimate (Blacknell, 1994, Dong 2004). Blacknell (2001) also proposes a parameter estimation method based on statistics of $x\log_{10}(x)$ and the results are said to be comparable to that of the moment ($\overline{x}$ and $\overline{z}$) method, but computationally less expensive.

To examine the accuracy of estimation schemes, datasets with known scale and shape parameters were generated. Since the correlation property (either temporal or spatial) of clutter is not involved in the above K distribution model, K-distributed clutter data, without considering its correlation property, can therefore be generated using (2) and (3) together. Figure 1 shows the pdf of the simulated data with the designated

distribution. The dataset contains $10^6$ samples with $\bar{x} = 0.3162$ ($20\log_{10}\bar{x} = -10dB$) and $\nu = 3.75$.

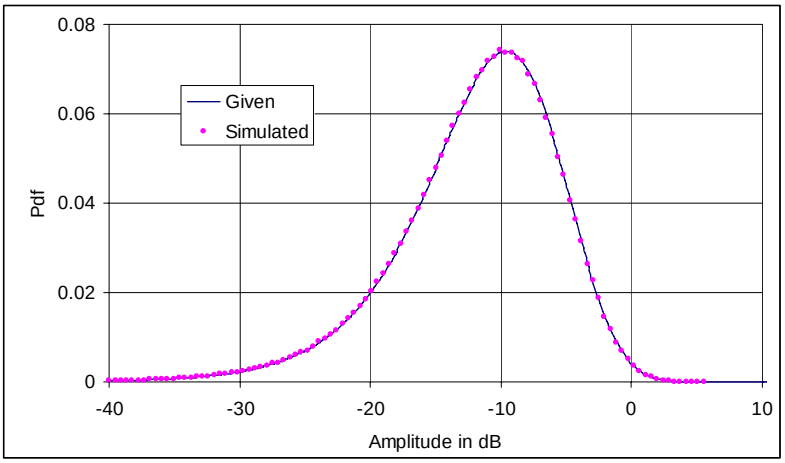


(a) pdf abscissa on linear scale to view global fit

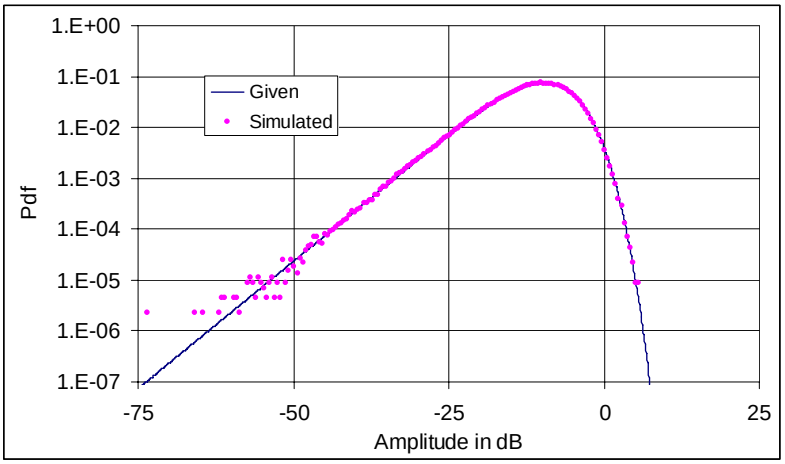


(b) pdf abscissa on log scale to view tail fit

*Figure 1: Simulation of the K distribution. The blue line is the pdf of the designated K distribution and the pink dots are the pdf of the simulated data.*

The accuracy of parameter estimation was quantitatively assessed using 100 simulations. In each simulation, the mean and the shape parameters were randomly generated, but confined within pre-defined ranges. In particular, the mean was

confined in the range of -20dB to 0dB[1], and the shape parameter was in the range of 0.3 to 5. The number of samples in each simulation was $10^6$.

The estimation accuracies for the mean and the shape parameter are shown in Figure 2 to Figure 4. We can see from Figure 2 that the mean estimation is accurate and stable, and the relative error is confined within $\pm 0.25\%$. Shown in Figure 3 is the shape parameter estimation using the first and second moments in the linear domain, i.e., (6) and (7). It can be seen that the estimation scheme is very unstable. While some estimates are at a relatively accurate level, other estimates are very poor and their relative error can be as large as $-100\%$. Figure 3 also shows that the estimation error tends to be biased, with the relative error being predominantly negative. The shape parameter estimation using the first moment in the linear domain and the first moment in the log domain, i.e., (6) and (9), is shown in Figure 4. The estimates of this scheme are stable and the relative errors are generally confined within $\pm 1\%$. It is also found that the absolute value of the relative error in Figure 4 is proportional to the value of the shape parameter. The larger the shape parameter, the larger the absolute value of the relative error in general. This is because as the shape parameter increases, the pdf become less and less sensitive to the shape parameter. Therefore, for cases with a large shape parameter, the estimation accuracy may be low, but the agreement between the estimated and data pdfs does not necessarily become poorer.

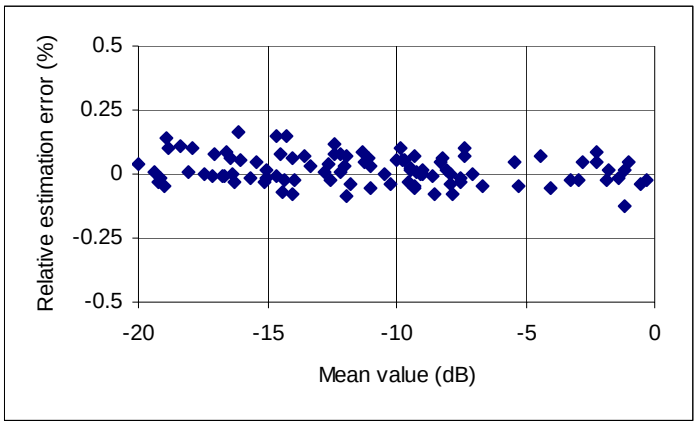


*Figure 2: The relative error of 100 mean estimates.*

[1] The mean is specified in the linear domain, but expressed in dB, that is, $20\log_{10}\bar{x}$, which is normally different from $\bar{z}$, the mean directly specified in the dB domain (refer to Table 1).

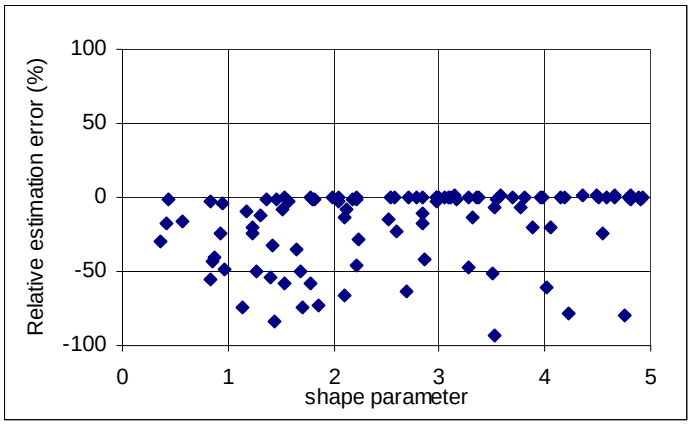


*Figure 3: The relative error of 100 shape parameter estimates using the first and second moments in the linear domain.*

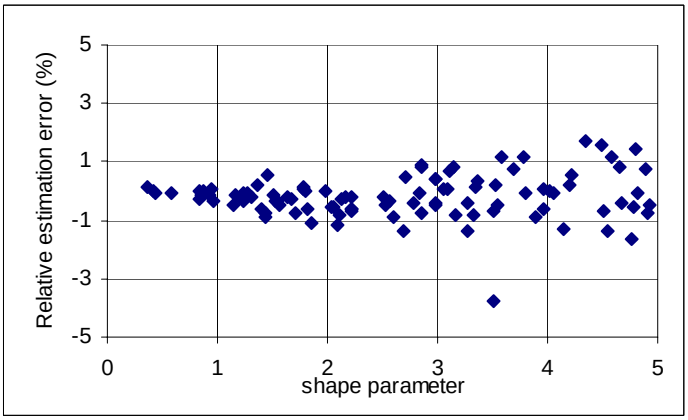


*Figure 4: The relative error of 100 shape parameter estimates using the first moment in the linear domain and the first moment in the log domains.*

It can be concluded from the above 100 simulations that the shape parameter estimation using the first moments in the linear and log domains, i.e., (6) and (9) together, is accurate and stable.

## 2.2 Distribution of the Sum of Uncorrelated K-distributed Samples

CFAR processors often utilise statistics of range cells surrounding the range CUT to determine if the CUT contains signals of targets. An example of such a processor is CA-CFAR, which adaptively sets a threshold by estimating the sum / mean level of a window of N range cells. Assuming that the global clutter distribution is the K-

distributed, we need to find the distribution of the sum of N such samples. In doing so we also assume that the range samples are uncorrelated.

For a K-distributed dataset with arbitrary shape parameter $\nu$, the distribution of the sum of N such samples cannot in general be expressed in closed form and has to be calculated numerically using the convolution method. For the special cases of the shape parameter $\nu = 0.5$, $\nu = 1.5$ and $\nu = m + 3/2$, $m = 1,2,\cdots$, closed-form expressions have been found (Armstrong and Griffiths, 1991).

For $\nu = 0.5$, the K-distribution (4) can be written as,

$$p(x) = c\exp(-cx) \tag{10}$$

which is a special case of the gamma distribution of (11) shown below with the shape parameter $a = 1$.

$$f(x) = \frac{c^a}{\Gamma(a)} x^{a-1} \exp(-cx) \tag{11}$$

It is well known that the distribution of the sum of $N$ independent gamma distributed samples with a shape parameter $a$ is still the gamma-distributed but with a shape parameter $Na$, as (Wilks, 1962),

$$f_N(x) = \frac{c^{Na}}{\Gamma(Na)} x^{Na-1} \exp(-cx) \tag{12}$$

Therefore, one can write the pdf of the sum of $N$ K-distributed samples with a global shape parameter $\nu = 0.5$, as,

$$p_N(x) = \frac{c}{\Gamma(N)} (cx)^{N-1} \exp(-cx) \tag{13}$$

For $\nu = 1.5$, we can derive,

$$p(x) = c^2 x\exp(-cx) \tag{14}$$

which is a case of the gamma distribution with the shape parameter $a = 2$. Therefore the pdf of the sum of N such samples is,

$$p_N(x) = \frac{c}{\Gamma(2N)} (cx)^{2N-1} \exp(-cx) \tag{15}$$

For $\nu = m + 3/2$, $m = 1, 2, \cdots$, the pdf of the sum of the N samples is given by (Armstrong and Griffiths, 1991),

$$p_N(x) = \gamma^N \exp(-cx) \sum_{j_0=0}^{N} \sum_{j_1=0}^{j_0} \sum_{j_2=0}^{j_1} \cdots \sum_{j_{m-1}=0}^{j_{m-2}} \binom{N}{j_0} \binom{j_0}{j_1} \binom{j_1}{j_2} \cdots \binom{j_{m-2}}{j_{m-1}} \times \frac{\beta_m^{N-j_0} \beta_{m-1}^{j_0-j_1} \cdots \beta_0^{j_{m-1}}}{\Gamma(2N + j_0 + j_1 + \cdots + j_{m-1})} (cx)^{2N-1+j_0+j_1+\cdots+j_{m-1}} \tag{16}$$

where

$$\gamma = \frac{c\sqrt{\pi}}{2^{m+1}\Gamma(\nu)} \tag{17}$$

$$\beta_i = \frac{(m+i)!(m+1-i)}{2^i\, i!} \tag{18}$$

To verify the correctness of (16), a simulated dataset was generated. The dataset contains $8 \times 10^6$ uncorrelated samples obeying the K distribution with a shape parameter $\nu = 5 + 3/2$, and a mean of $\bar{x} = 1.0$. The pdf of the dataset and its theoretical pdf are shown in Figure 5 (the left distribution). The dataset was then regrouped to $10^6$ samples and each was the sum of 8 original samples ($N = 8$). The pdf of the regrouped dataset and its theoretical pdf are also shown in Figure 5 (the right distribution). The agreement between the pdfs confirms the correctness of (16).

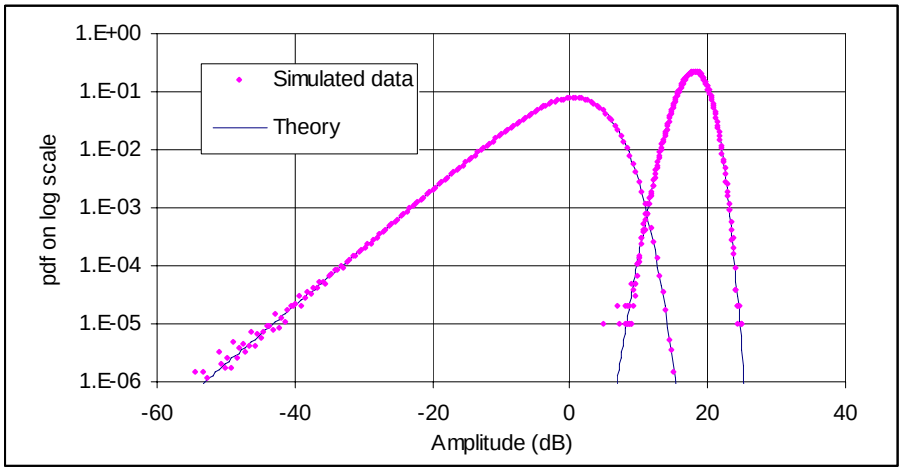


*Figure 5: Two simulated distributions (pink dots) and their theoretical distributions (blue lines). The left distribution is of a K-distributed dataset with a shape parameter of 6.5. The right one is the distribution of the sum of 8 original samples.*

# 3. Weibull Distribution

## 3.1 Weibull Distribution

Sea clutter data are also reported to be Weibull distributed (Billingsley, 2002, Long 2001). The pdf of a Weibull distribution is given as,

$$p(x) = bcx^{b-1}\exp(-cx^b) \qquad x > 0 \tag{19}$$

where $b$ is the shape parameter and $c$ is the scale parameter[2]. The properties of the Weibull distribution can be found elsewhere (Billingsley, 2002, Dong, 2004), and Table 2 lists the main properties of the Weibull distribution.

There are two special cases where the Weibull distribution is identical to the K distribution. One case is $b = 2$ for the Weibull distribution and $\nu = \infty$ for the K distribution, in this case both distributions are identical to the Rayleigh distribution. Theoretically, the distribution of sea clutter data cannot be better than the Rayleigh distribution, therefore $b = 2$ should be the upper boundary if sea clutter distribution is fitted by the Weibull distribution. Another case is $b = 1$ for the Weibull distribution and $\nu = 0.5$ for the K distribution, in this case the two distributions are identical to the gamma distribution (Dong, 2004)[3]. The range $1 < b < 2$ for the Weibull distribution corresponds to the range $0.5 < \nu < \infty$ for the K distribution. Another interesting point is that in the range $b < 1$ $(\nu < 0.5)$ the K- distribution converges faster than the Weibull distribution (the tail of the K distribution is shorter) whereas in the range $1 < b < 2$ $(0.5 < \nu < \infty)$ the K distribution converges more slowly than the Weibull distribution (the tail of the K distribution is longer) (Dong, 2004). High grazing angle sea clutter data collected by the Ingara system is found normally in the $1 < b < 2$ range (refer to Section 4)[4], therefore the convergence of the K distribution fit is normally slower than that of the Weibull distribution fit.

---

[2] To be consistent with literature, symbols $c$ and $b$ are used in both the K and Weibull distributions. However, there should be no confusion from the context.

[3] In Dong's report (2004), the pdf of intensity was discussed. Therefore the two cases are (1) $b = 1$ for the Weibull distribution and $\nu = \infty$ for the K distribution and (2) $b = 0.5$ for the Weibull distribution and $\nu = 0.5$ for the K distribution.

[4] The case of $b < 1$ $(\nu < 0.5)$ for sea clutter at low grazing angles has been reported, see Watts et al (2005).

*Table 2: Statistics of the Weibull distribution in the linear and log domains:*

| Property | Linear domain | Log domain |
|---|---|---|
| Pdf | $p(x) = bcx^{b-1}\exp(-cx^b)$ | $p(z) = k_0 bc10^{zb/20}\exp(-c10^{zb/20})$ |
| Cdf | $P(x<t) = 1-\exp(-ct^b)$ | $P(z<t) = 1-\exp(-c10^{tb/20})$ |
| First moment | $\bar{x} = \frac{\Gamma(1+1/b)}{c^{1/b}}$ | $\bar{z} = -\frac{1}{k_0 b}(\psi^{(0)}(1)+\ln c)$ |
| Second moment | $\overline{x^2} = \frac{\Gamma(1+2/b)}{\Gamma^2(1+1/b)}\bar{x}^2$ | $\overline{z^2} = \frac{\pi^2}{6k_0^2 b^2}+\bar{z}^2$ |

The ML parameter estimates for the Weibull distribution exist in an iterative solution which involves data samples and is computationally expensive. (Oliver, 1993, Dong, 2004),

Similarly, the estimation using the first moment in the linear domain and the first moment in the log domain provides stable results very close to the ML estimates.

## 3.2 Transformation between Weibull and Rayleigh, Weibull and Gamm Distributions

A Weibull distribution with arbitrary parameters can be transformed to a Rayleigh or a gamma distribution and vice versa. The significant advantage of such transformation is that the statistics and characteristics of the Rayleigh distribution are well known, and radar performance and target detection schemes such as CFAR under the Rayleigh environment have been well studied, documented and implemented in radar systems. Supposing that $x$ is Weibull distributed and whose pdf is given in (19), let

$$x = \left(\frac{t^2}{2cs^2}\right)^{1/b} \tag{20}$$

we have

$$p(t) = p\big(x(t)\big)\left|\frac{dx}{dt}\right| = \frac{t}{s^2}\exp\left(-\frac{t^2}{2s^2}\right) \qquad t>0 \tag{21}$$

It is well known that $p(t)$ is a Rayleigh distribution for the amplitude of a complex variable whose real and imaginary parts are mutually uncorrelated and each obeys a normal distribution with zero mean and standard deviation of $s$, designated as $N(0,s)$. It is not difficult to calculate,

$$\bar{t} = \int_0^\infty tp(t)dt = s\sqrt{\pi/2} \tag{22}$$

and

$$\overline{t^2} = \int_0^\infty t^2 p(t)dt = 2s^2 \tag{23}$$

Based on the above derivation, any dataset having a Weibull distribution can be transformed to a Rayleigh distribution and vice versa using the mapping function (20) provided that parameters $b$ and $c$ are known or have been estimated. To demonstrate, a dataset comprised of $10^6$ complex samples was generated. The real and imaginary parts of samples are uncorrelated but each part obeys the normal distribution with zero mean and standard deviation of $s = 1/\sqrt{\pi/2}$. We then chose $b = 1/2$ and $c = \Gamma^b(1+1/b)$ (the selection of these parameters makes $\bar{t} = 1$ for the Rayleigh distribution and $\bar{x} = 1$ for the Weibull distribution) to transform the data using (20). The distributions of simulated data before and after the transformation, as well as the theoretical Rayleigh and Weibull distributions are plotted in Figure 6. It can be seen that the Rayleigh distributed data are now transformed to the Weibull distributed data.

Letting $t = x^b$, we transform the Weibull distribution (19) to the gamma distribution (10). The detailed simulation for this transformation is omitted.

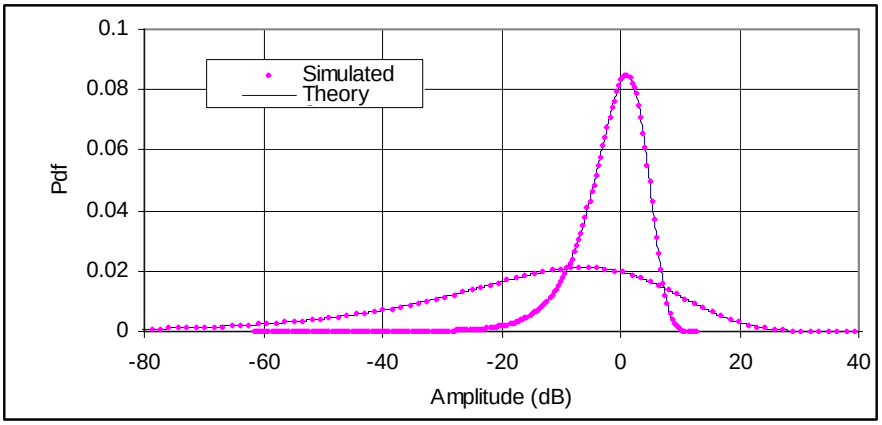


(a) pdf abscissa on linear scale to view global fit

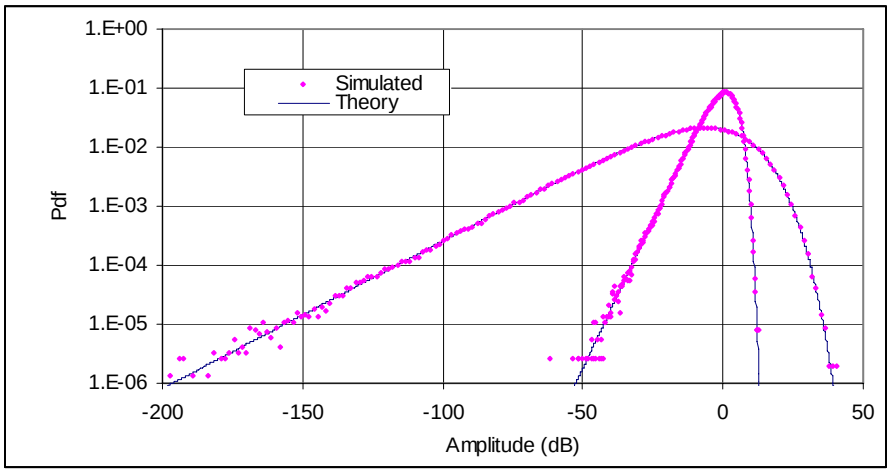


(b) pdf abscissa on log scale to view tail fit

*Figure 6: Simulated Rayleigh distribution (the narrow one) and its transformation to the Weibull distribution (the wide one). The blue lines and pink dots correspond to the distributions of theory and the distributions of simulated data.*

## 3.3 Distribution of the Sum of Uncorrelated Weibull Distributed Samples

Statistical properties of the Weibull distribution and their applications particularly in CFAR schemes have been widely discussed (Anastassopoulos and Lampropoulos, 1995, Levanon and Shor, 1990, Sekine and Mao, 1990). Letting $t = x^b$ we transform the Weibull distribution (19) to the gamma distribution (11) with the shape parameter of 1. The distribution of the sum of N transformed samples is therefore,

$$p_N(t) = \frac{c^N}{\Gamma(N)} t^{N-1} \exp(-ct) \tag{24}$$

The equation (24) applies only to the transformed data.

The distribution of the sum of the Weibull distributed data cannot in general be expressed in closed-form, because the integral below does not have closed form for an arbitrary shape parameter $b$.

$$p_N(t) = \int_0^t p(t-x)\, p_{N-1}(x) dx \tag{25}$$

where $N = 2, 3, \cdots$, and $p_1(x) = p(x)$

We propose a formula for the distribution of the sum of Weibull distributed data in (26). Since the close-form formula is not existed, the proposed formula (26) is only an approximation.

$$p_N(x) = \frac{r\, bc^N}{\Gamma(N)} (r\, x)^{Nb-1} \exp(-c(r\, x)^b) \tag{26}$$

where

$$r = \frac{\Gamma(N + 1/b)}{N\, \Gamma(N)\Gamma(1 + 1/b)} \tag{27}$$

The parameter $r$ can be considered as a scale parameter, so that the first moment (the mean) of the distribution (26) is equal to the mean of the sum of the N Weibull distributed data.

The first moment of (26) is,

$$\mu = \int_0^\infty x p_N(x) dx = \frac{\Gamma(N + 1/b)}{r\, \Gamma(N) c^{1/b}} \tag{28}$$

The mean of the sum of the N Weibull distributed samples is (refer to Table 2) $N\bar{x} = N\, \Gamma(1 + 1/b) c^{-1/b}$. Letting $\mu = N\bar{x}$ results in (27).

Except for the special case of $b = 1$ when the Weibull distribution is identical to the gamma distribution (11), the derivation of (26) cannot be established. As we know that there is no closed form for the distribution of the sum of Weibull distributed samples, the proposed formula is therefore at most an approximation. The remaining questions

are that firstly if the expression of (26) is rational and secondly how big the error is between the proposed formula and the true distribution. To answer the first question, we notice that the Weibull distribution (19) is a generalised gamma distribution, and therefore, the distribution of the sum of Weibull distributed samples should also be a generalised gamma distribution. The expression of (26) is indeed a generalised gamma distribution. To answer the second question, the error may be evaluated by comparing the result of (26) and the numerical evaluation of (25), representing the true distribution. The numerical evaluation of (25) is also referred to as the convolution method, as the integral has the convolution form (Wilks, 1962). Figure 7 compares the results of (25) and (26) with $b = 1.345$, $\bar{x} = 0.123$, $N = 2$ and $N = 8$. It can be seen that the two pdfs convoluted using (25) and the two pdfs calculated using the proposed formula (26) are virtually identical even in the very far tail region for both cases.

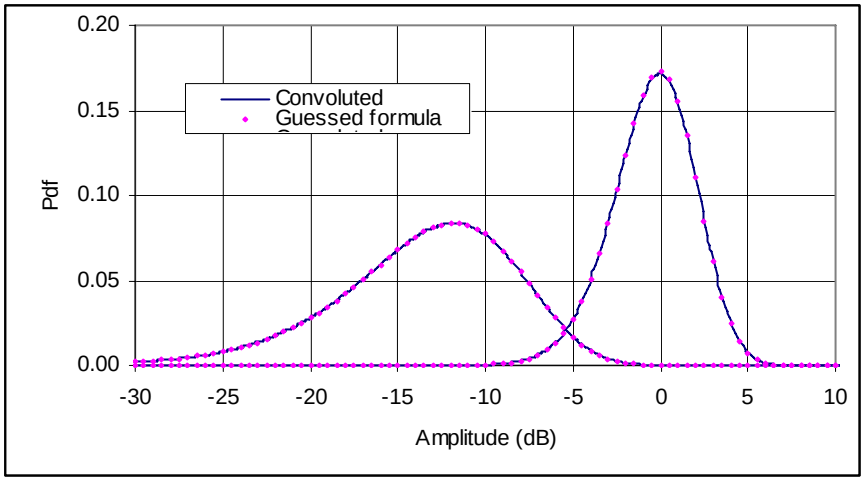


(a) pdf on the linear scale to view the global agreement

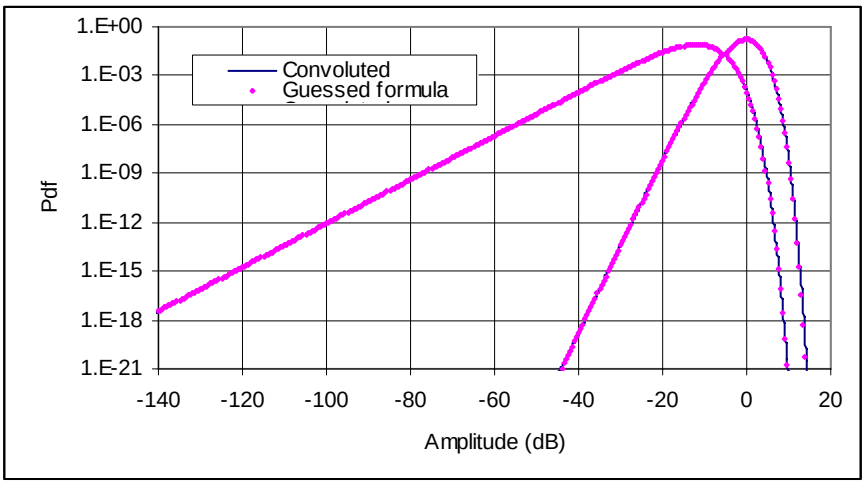


(b) pdf on the log scale to view the tail agreement

*Figure 7: Two distributions are the pdfs of the sum of 2 (the left distribution) and the sum of 8 (the right distribution) Weibull distributed samples. The blue lines and pink dots correspond to (25) and (26), respectively.*

To further confirm the correctness of (26), we show below two examples using simulated data. In the first example, we let $b = 1.345$ (recall that $1 < b < 2$ for the Weibull distribution corresponds to $0.5 < \nu < \infty$ for the K distribution) and $\bar{x} = 0.123$. The original Weibull distributed dataset contained $10 \times 10^6$ samples. The data were regrouped in to $10^6$ samples and each was the sum of 10 original samples ($N = 10$). The two distributions, one for the original Weibull distributed data and the other for

the sum of 10 original samples are shown in Figure 8. The second example used the following parameters: $b = 0.65$ (recall that $b < 1$ for the Weibull distribution corresponds to $\nu < 0.5$ for the K distribution) and $\bar{x} = 0.123$. The original datasets contained $5 \times 10^6$ samples, which were then regrouped to $10^6$ samples and each was the sum of 5 original samples ($N = 5$). The corresponding distributions are shown in Figure 9. With the support of these two examples we can accept (26) as a very good approach to the close-form for the distribution of the sum of Weibull distributed data. The error between (26) and numerical results of (25) is too small to be observed in the range of interest.

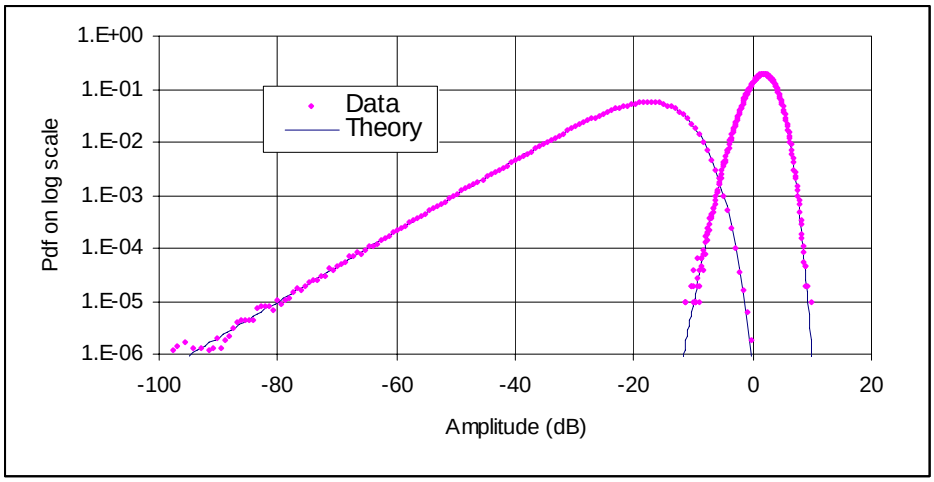


*Figure 8: Two distributions of Example 1. The left and right distributions are for the original Weibull distributed samples and the sum of 10 original samples, respectively. In each distribution, the pink dots and the blue lines represent the data distributions and the theoretical distributions, respectively.*

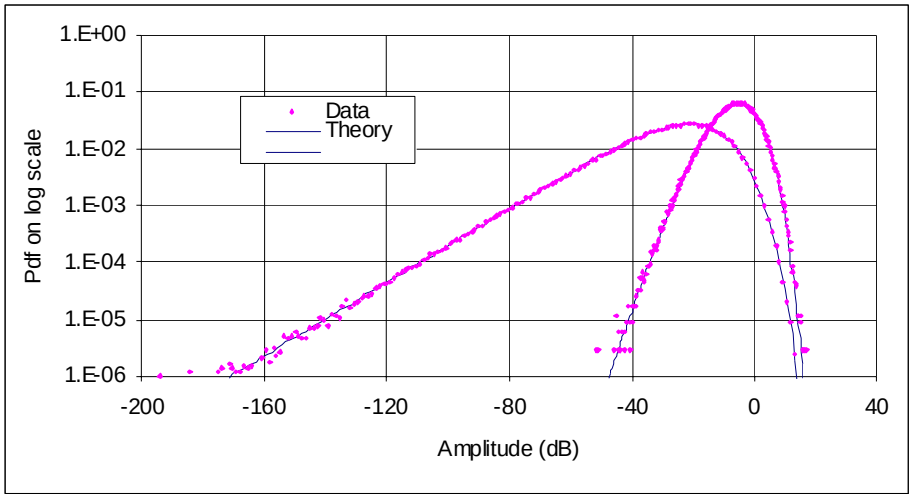


*Figure 9: Two distributions of Example 2. The left and right distributions are for the original Weibull distributed samples and the sum of 5 original samples, respectively. In each distribution, the pink dots and the blue lines represent the data distributions and the theoretical distributions, respectively.*

## 3.4 CA CFAR Threshold

Using (26) we can determine the threshold $T$ used in CA CFAR detection scheme by the following integral,

$$P_{fa} = \int_0^\infty P(X_0 \geq TX)\, p_N(x)dx = \int_0^\infty \exp[-c(Tx)^b]\, p_N(x)dx \tag{29}$$

Consequently, (29) after some manipulations becomes

$$P_{fa} = \frac{1}{\left[1+\left(T/r\right)^b\right]^N} \tag{30}$$

where $N$ is the size of the process window. Obviously if $b=1$, (30) simplifies to the well-known formula,

$$P_{fa} = \frac{1}{\left[1+T\right]^N} \tag{31}$$

An Optimal Weibull (OW) CFAR, in the maximum likelihood sense, for Weibull distributed clutter has been proposed (Anastassopoulos and Lampropoulos, 1995). The proposed estimator is derived through the distribution of a new variable $t$ defined as,

$$t = \xi \left[ \frac{1}{N} \sum_{i=1}^{N} x_i^b \right]^{1/b} \tag{32}$$

where $\xi = \Gamma(1+1/b)$.

The threshold $T_{ow}$ of the proposed estimator is given by,

$$P_{fa} = \frac{1}{\left[ 1 + \frac{(T_{ow}\xi)^b}{N} \right]^N} \tag{33}$$

The OW-CFAR estimator works in the following way. For given false-alarm rate $P_{fa}$, window size $N$ and shape parameter $b$, the threshold $T_{ow}$ is determined. For each CUT $x$, the value of $t$ for the companioned window is computed. If $x > T_{ow} t$, target presence is declared and vice versa.

Using the Monte Carlo simulation method, we compared the proposed CA-CFAR detector to the OW-CFAR detector. We generated a Weibull distributed dataset containing one million samples with an random shape parameter confined in the range of $0.5 \le b \le 2$. The false-alarm rate was set to $P_{fa} = 10^{-4}$ and the window size was 24 and 32, respectively. The actual false-alarm rate was calculated via test of all samples. The simulation was repeated 100 times and the results are shown in Figure 10. It can be seen that the two estimators performs approximately the same. However, the proposed CA-CFAR is much simpler as it only requires the sum over the window, whereas the OW-CFAR invokes nonlinear manipulation of the window as indicated in (32).

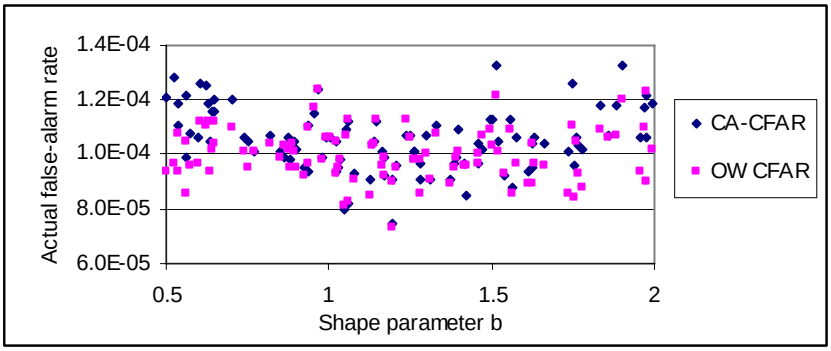


(a) $N = 24$

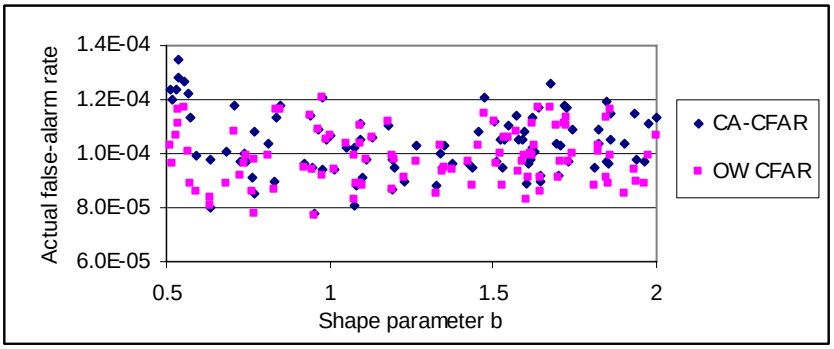


(b) $N = 32$

*Figure 10: Actual false-alarm rates of CA-CFAR and OW-CFAR estimators in the environment of Weibull clutter. The false-alarm rate was set to $10^{-4}$.*

# 4. Sea Clutter Data Analysis

Extensive X-band sea clutter data has been collected at high grazing angles in the Sea Clutter Trial 2004 (SCT04) from the Southern Ocean approximately 100km south of Port Lincoln, South Australia in August 2004, using the DSTO developed airborne X-band fully polarised radar system, Ingara. Details of the trial and some data analysis can be found in the DSTO report, DSTO-TR-1818 (Crisp et al, 2006).

## 4.1 Dataset Descriptions

The SCT04 trial collected data at the incidence angle approximately varying from $45^{o}$ to $80^{o}$ on 8 separate days in a period of 18 days. This report primarily studies the datasets

of run34683 and run34690, collected on 16/08/04 at approximately 10:52am to 11:27am local time, and processed as real aperture data. The radar was operated in the circular spotlight mode, and therefore, it can be considered that the radar looked at approximately the same spot of the sea surface but at different incidence angles (different runs) and different azimuth angles (same run but different datasets). Each run has a nominal incidence angle and consists of about 72 datasets to cover the whole $360^o$ azimuth angles. Each dataset which was processed to cover an azimuth angle span of $5^o$, contains approximately 920 pulses, and the number of the range compressed samples is 1024 at a range resolution of 0.75m. Therefore each dataset, which contains about $920 \times 1024$ samples, has a slant range coverage of 750m, corresponding to a incidence angle span of $3.5^o$ to $8^o$ depending on the nominal incidence angles, and an azimuth angle span of $5^o$. Table 3 lists some radar parameters used in the SCT04.

*Table 3: Radar parameters*

| Parameter | Value |
|---|---|
| Centre frequency | 10.1 GHz |
| Bandwidth of LFM | 200 MHz |
| Polarisation | Full |
| Pulse width | 20 μs |
| Altitude | 2314 m for nominal incidence angle of $50^o$<br>1353 m for nominal incidence angle of $70^o$ |
| Incidence angle | $51.3^o$ for run34683 and $67.2^o$ for run34690 |

## 4.2 Wind and Wave Ground-Truth

Wind and wave ground-truth data were collected during the SCT04 trial and details have been reported (Crisp et al, 2006). The wind and wave parameters on the day of 16/08/04 at the approximate clutter collection time are shown in Table 4 and Table 5, respectively. These parameters are retrieved from the Australian Government Bureau of Meteorology (BoM) Automatic Weather Station (AWS) data and a wave buoy deployed near the site. It can be seen that the wave direction and the wind direction are significantly separated from each other and this is in fact not uncommon. The sea state is dependent on both the swell and the local wind waves. The swell is generated by distant storms or a constant wind blowing for long duration and fetching a long distance (Skolnik, 2001, Chapt 7). The swell is therefore not related to the local wind directions. The wave information in Table 5 probably reflects the swell rather than the wind waves.

*Table 4: Wind speed and direction at the mid-data collection time.*

| Date | Wind speed (m/s) | | Wind direction(°) | |
|---|---|---|---|---|
| | AWS | BoM model | AWS | BoM model |
| 16/08/04 | 9.3 | 7.1 | 68 | 47 |

*Table 5: Wave height and direction at the mid-data collection time.*

| Date | Wave height (m) | | Wave direction(°) | |
|---|---|---|---|---|
| | Buoy | BoM model | Buoy | BoM model |
| 16/08/04 | 2.5 | 2.4 | 169 | 211 |

## 4.3 Sea Clutter as a Function of Azimuth Angle

It is well known that sea clutter is a function of azimuth angle even if other parameters remain unchanged (Ulaby et al, 1982, p. 855). Clutter in the upwind direction is strongest. The weakest clutter is either in the downwind or crosswind direction, depending on the sea surface conditions and the radar parameters (Skolnik, 2001, Chapt 7). The mean of the sea clutter of run34683 and run34690 is shown in Figure 11. It can be seen that the first and second peaks are approximately in agreement with the upwind and downwind directions, respectively, and valleys with the crosswind direction[5]. It is seen that the HH clutter is about 4-7dB lower than the VV clutter and the HV clutter is further about 5-10dB down regardless of azimuth angles. It is also seen by comparing Figure 11 (a) and Figure 11 (b) that the clutter decreases with the increase in incidence angle (decrease in grazing angle).

[5] The azimuth angle of Ingara is defined as the angle the radar looks from. The upwind direction is the direction the wind blows from. Therefore the angle of the wind direction shown in Table 4 plus 180° would be the angle the radar looks to the upwind direction.

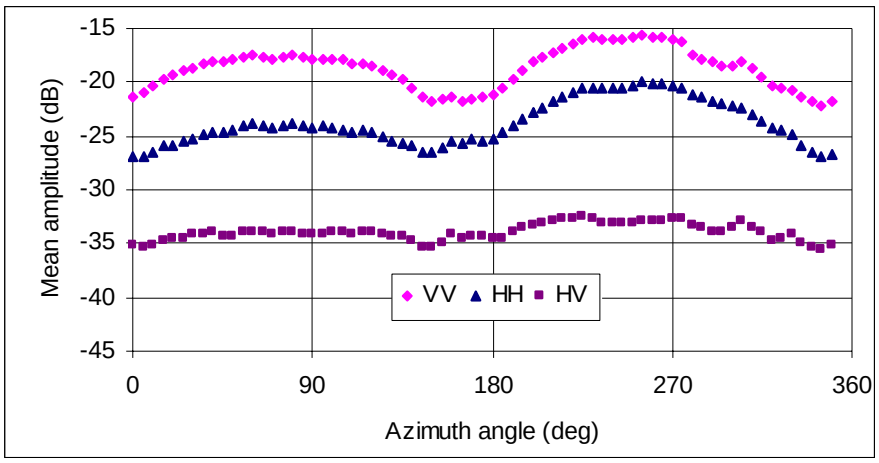


(a) run34683 with an incidence angle of 51.2°

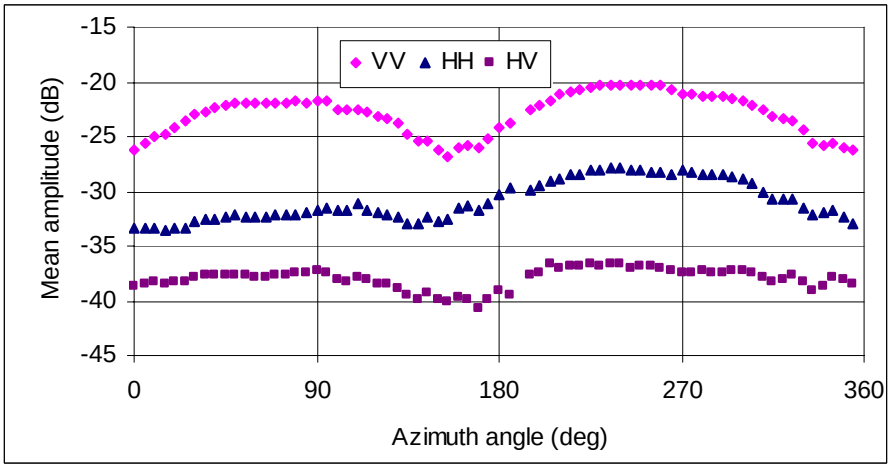


(b) run34690 with an incidence angle of 67.2°

*Figure 11: Sea clutter as a function of azimuth angle for datasets of (a) run34683 and (b) run34690. The first and second peaks are approximately in agreement with the upwind and downwind directions, respectively, and the valleys with the crosswind direction.*

The estimated shape parameter $\nu$ of the K distribution for these two runs is shown in Figure 12. It can be seen that the HH clutter is normally spikier than the VV clutter as the $\nu$ parameter for the HH clutter is usually smaller. The $\nu$ parameter for the HV clutter is in between indicating that the HV clutter is not as spiky as the HH clutter, but spikier than the VV clutter. It is also seen that the shape parameter does not show a clear azimuth pattern as the clutter amplitude, which means that although clutter tends

to be strongest in the upwind direction, it is not necessarily spikiest. It should be pointed out that the bigger fluctuation in $\nu$ parameter for the VV data does not mean that the variation in VV clutter distribution with respect to the azimuth angle is more serious. In fact it is simply because the variation of a K distribution becomes less and less sensitive to large values of $\nu$. This can be further verified by viewing Figure 13 which shows the estimated $b$ parameter of the Weibull distribution for these two datasets. Fluctuations of the estimated $b$ parameter of the Weibull distribution with respect to azimuth angle for HH, VV and HV polarisations are all about the same. The estimated parameter $b$ falls in the range of $1 < b < 2$ for all datasets indicating that estimated Weibull distribution will converge a little faster than the estimated K distribution for all datasets.

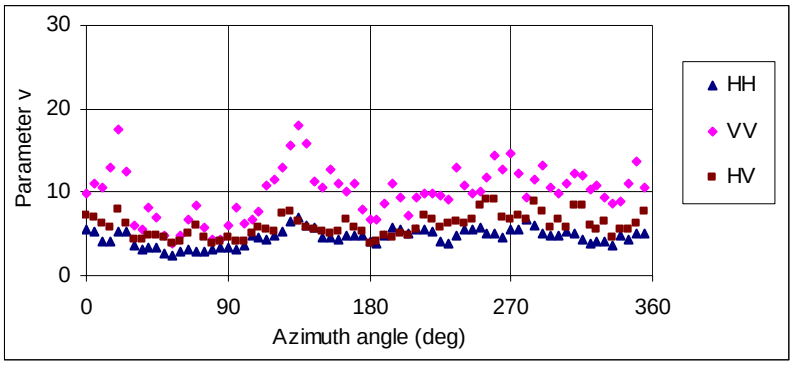


(a) run34683

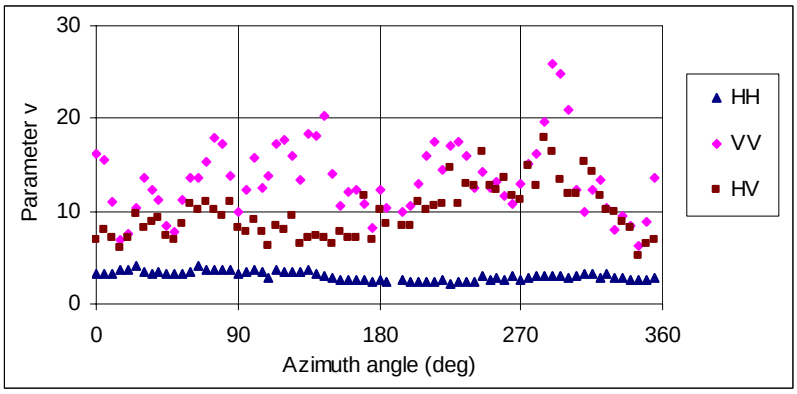


(b) run34690

*Figure 12: The estimated parameter $\nu$ of the K distribution for datasets run23683 and run34690.*

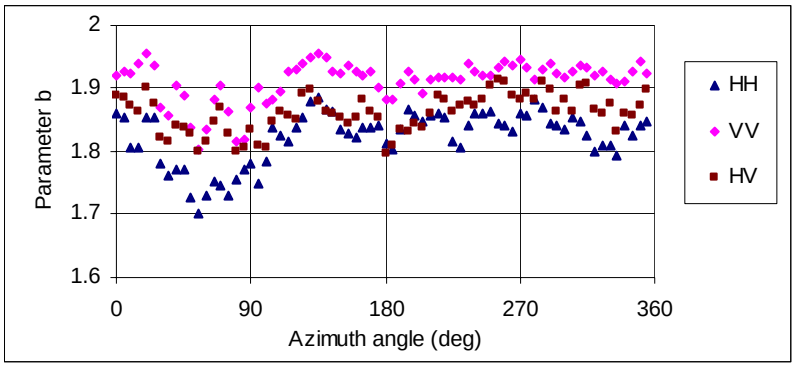


(a) run34683

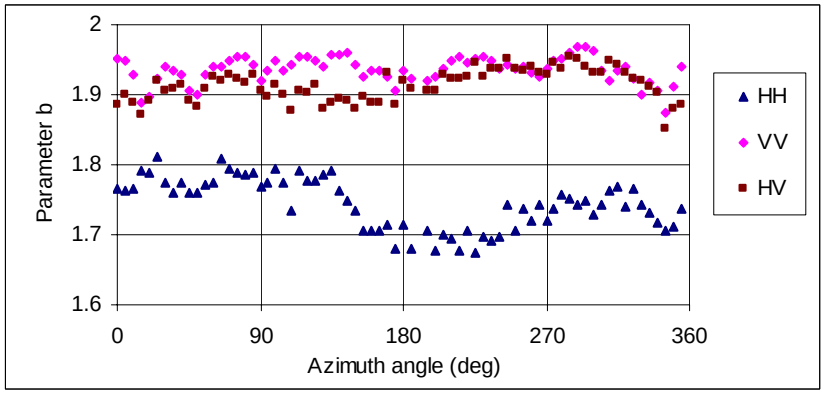


(b) run34690

*Figure 13: The estimated parameter $b$ of the Weibull distribution for datasets of run34683 and run34690.*

## 4.4 Discrepancies between Data and Fitted Distributions

As discussed previously, the K or Weibull distribution is commonly found to be a good fit to sea clutter spatial distributions. Supposing that parameters of the clutter distribution are estimated for a given clutter environment, the performance of the target detection scheme under the clutter environment will then depend on the estimated parameters. Because the fitted distribution is not the true distribution of the dataset, we have to look at the disagreement between the two, especially in the tail region from the perspective of target detection. We need to estimate the possible errors between the two in order to have a good estimate of the radar performance. We calculated the discrepancy between the data cdf and the modelled cdf in the tail region to quantitatively determine the difference between the two. We found that the distribution of the sea clutter data collected by the Ingara system is not always in good

agreement with the fitted either K or Weibull distribution particularly for the HH data in the region beyond cdf > 0.999. Depending on the nature of the dataset, some can be well fitted by either the K or Weibull distribution and others cannot.

Figure 14 and Figure 15 show two examples of the pdf fit. These two examples are purposely chosen in such a way that a good fit is observed in Figure 14 whereas a bad fit is seen in Figure 15. It can be seen in the good fit example that the fitted K distribution follows the data distribution beautifully even in the far tail region. On the other hand, in the bad fit example the data distribution suddenly departs from the fitted distribution in the far tail region.

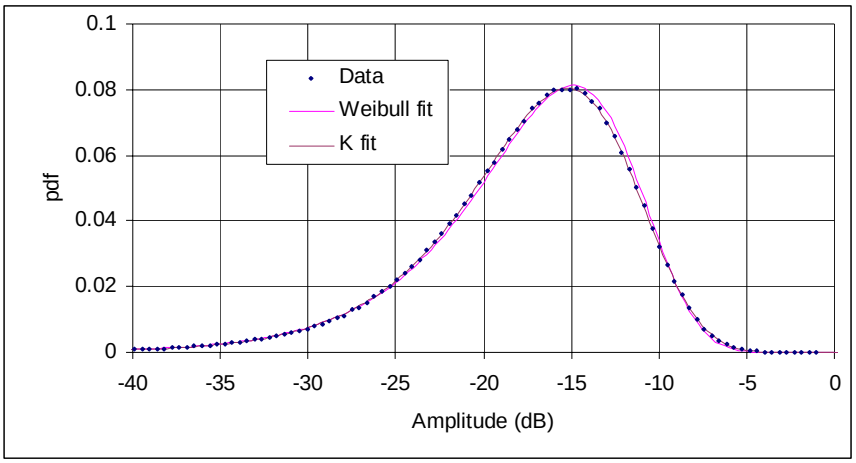


(a) pdf abscissa on linear scale to view global fit

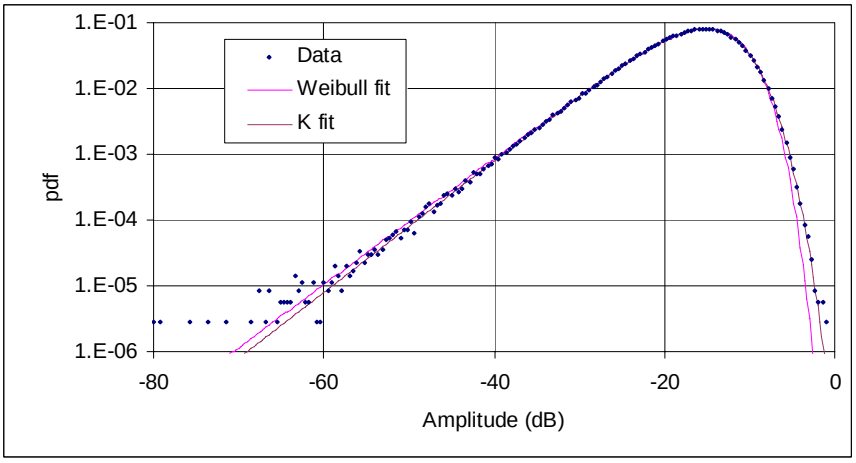


(b) pdf abscissa on log scale to view tail fit

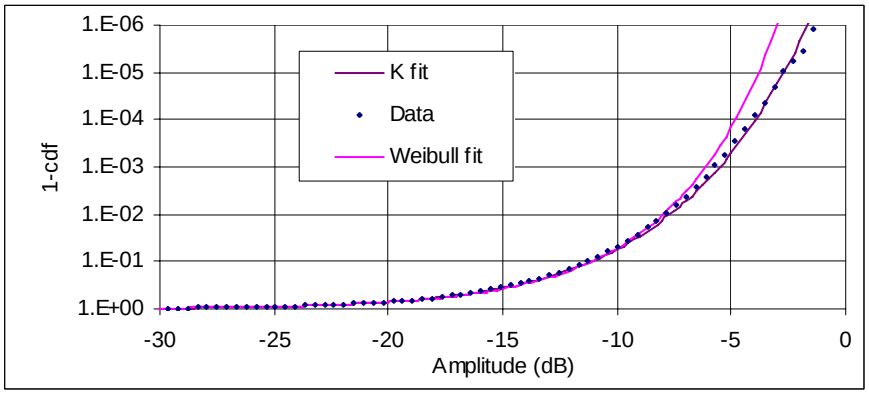


(c) 1-cdf abscissa on log scale to view cdf convergence

*Figure 14: The K and Weibull distribution fits for the VV polarised data of run34683_rccal_225 (an example of good fit). The Weibull fit is not as good as the K fit.*

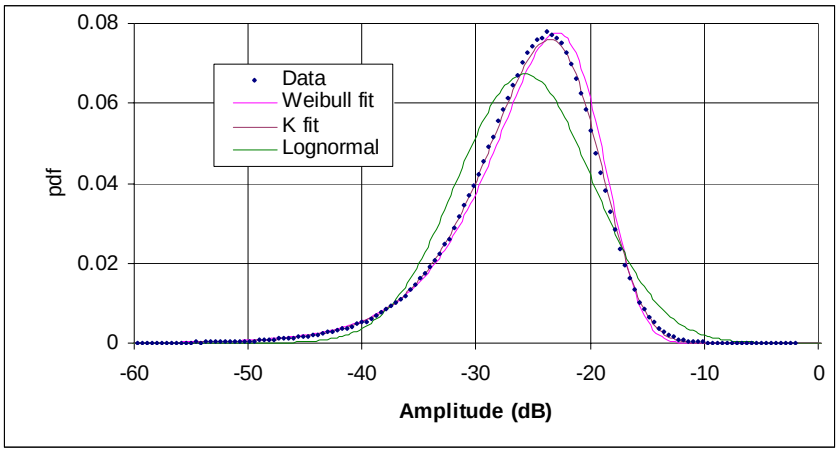


(a) pdf abscissa on linear scale to view global fit

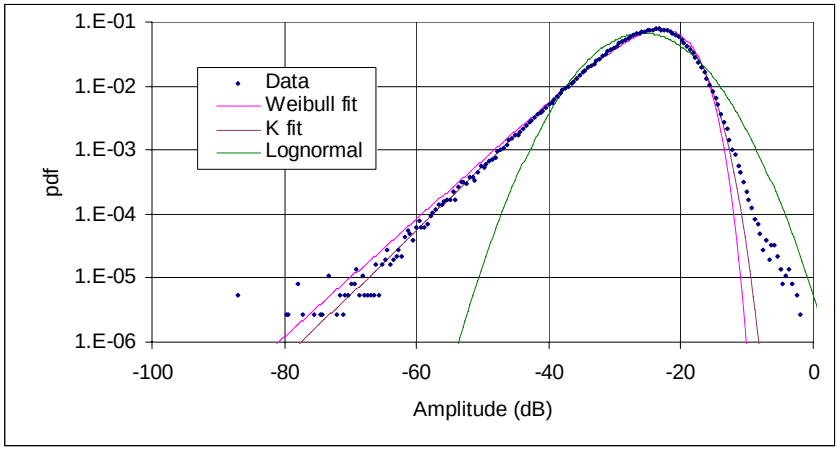


(b) pdf abscissa on log scale to view tail fit

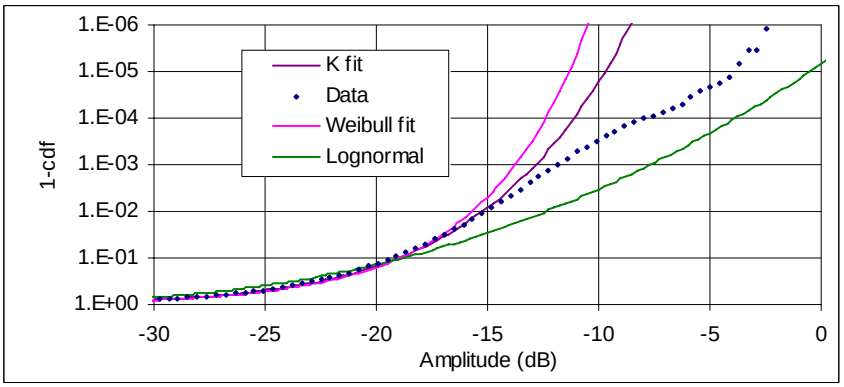


(c) 1-cdf abscissa on log scale to view cdf convergence

*Figure 15: The K, Weibull and lognormal distribution fits for the HH polarised data of run34683_rccal_190 (an example of bad fit). None of the three models is in good agreement with the data distribution in the far tail region.*

To quantitatively assess the agreement between the fitted distribution and the data distribution in the tail region, the difference (or separation) measured in dB between the fitted cdf and the actual cdf for the HH, VV and HV data at 1-cdf equal to $10^{-3}$ and $10^{-5}$ was calculated and shown in Figure 16 to Figure 19. For instance, the amplitudes at the 1-cdf equal to $10^{-5}$ level are −9.75dB and −4.05dB for the fitted K distribution and the HH distribution, respectively, as shown in Figure 15 (c), the difference for this case is therefore, $-9.75-(-4.05)=-5.7$ dB. Viewing these figures, we observe,

- Overall the K distribution provides the best fit for the VV data. The error between the fitted K cdf and data cdf is less than −0.5dB at the $10^{-3}$ level and about −1.5dB at the $10^{-5}$ level for the VV data.

- The biggest error between the fitted K cdf and data cdf at the $10^{-5}$ level can be up to −5 to −7dB for the HH data. This is attributed to the data distribution suddenly departing from the fitted distribution as seen in Figure 15.

- The error for the HV data fit is in between, i.e., the error is not as small as that of the VV data, but not as big as that of the HH data either.

- Among the three commonly used distributions (including the lognormal distribution[6]), the K distribution is the best fit, followed by the Weibull distribution for the data studied. It is found that the fitted Weibull distribution converges a little faster than the fitted K distribution which in turn converges a little faster than the data distribution. The overall fit of the lognormal distribution is not good and its convergence is usually too slow compared to that of the clutter data.

In summary, we observe the sea clutter distribution can be fitted with the K distribution or Weibull distribution with a reasonable high accuracy at the level of 1-cdf equal to $10^{-3}$ or lower. However, at the $10^{-4}$ level or higher, the pdf of some datasets deviates from the K- or Weibull distribution. The biggest difference between the fitted cdf and the data cdf is normally found for the HH data, due to its spikiest nature.

The impact of clutter distribution fit errors is that any detection performance modelling or target detection algorithm that uses or assumes a particular distribution (e.g. K) in setting the detection threshold for a desired false alarm rate (typically around the $10^{-5}/10^{-6}$ level), will actually be setting the threshold too low and therefore result in a much higher number of false alarms than expected.

[6] We omit details of the log-normal distribution, as it is the worst fit for the sea clutter studied. Interested readers may refer to Long (2001) for more details of the lognormal distribution.

We present better distribution models in the following Sections.

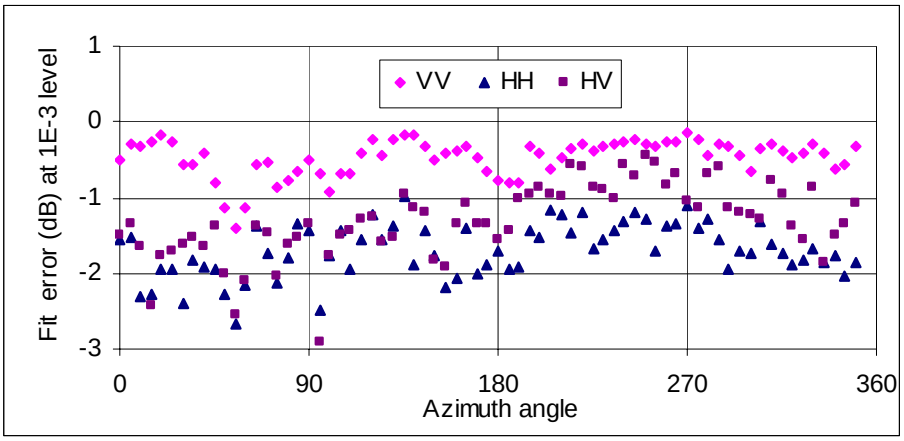


(a) Weibull fit

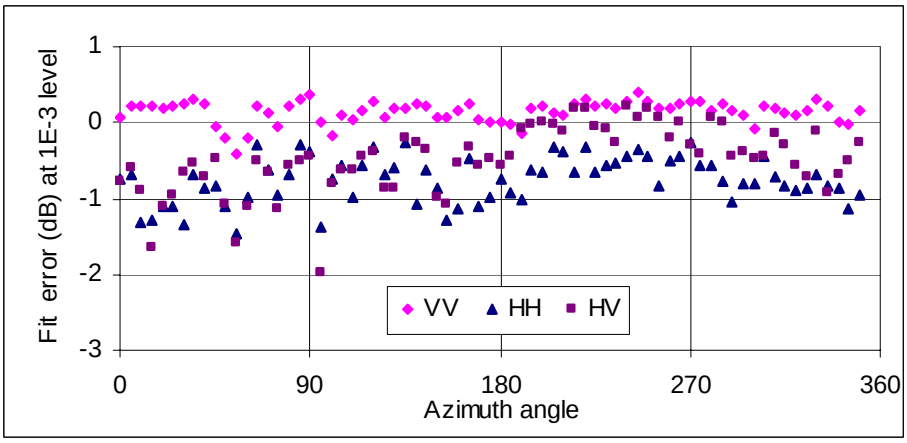


(b) K fit

*Figure 16: Difference in dB between the fitted cdf and the actual cdf at 1-cdf equal to $10^{-3}$ for datasets of run34683.*

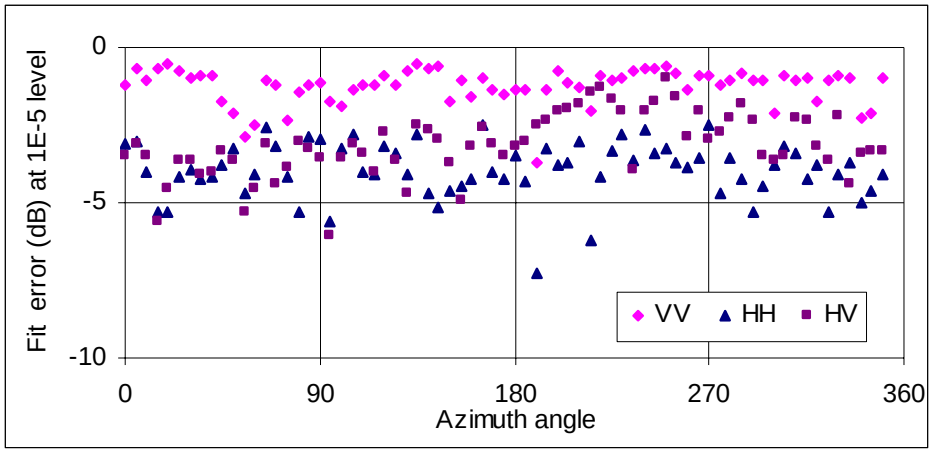


(a) Weibull fit

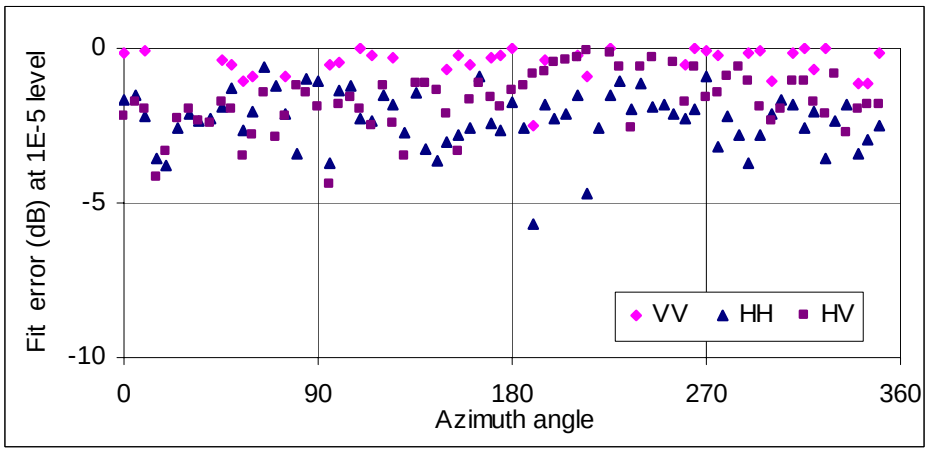


(b) K fit

*Figure 17: Difference in dB between the fitted cdf and the actual cdf at 1-cdf equal to $10^{-5}$ for datasets 34683.*

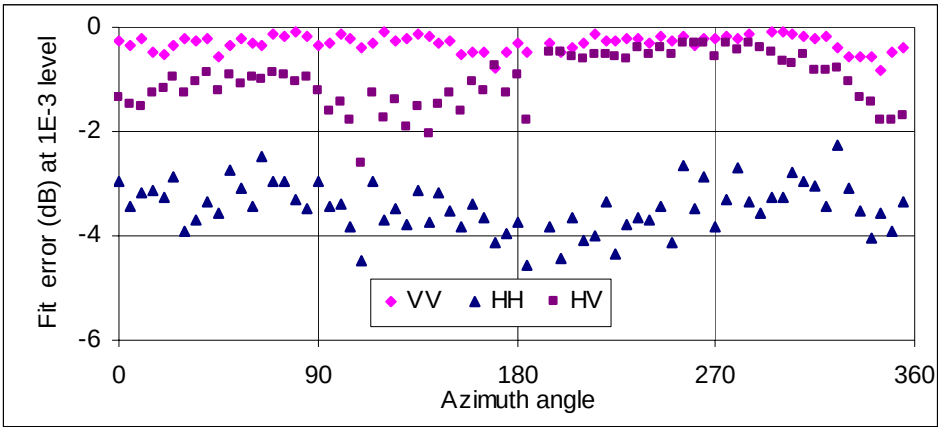


(a) Weibull fit

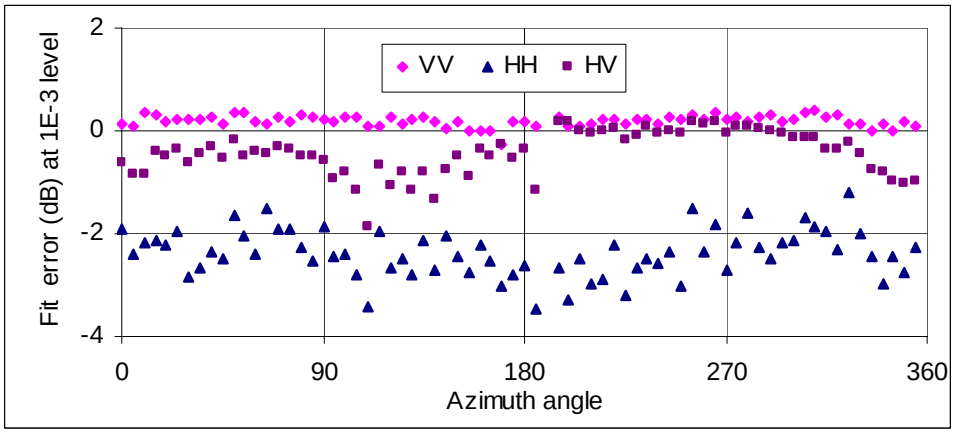


(b) K fit

*Figure 18: Difference in dB between the fitted cdf and the actual cdf at 1-cdf equal to $10^{-3}$ for datasets of run34690.*

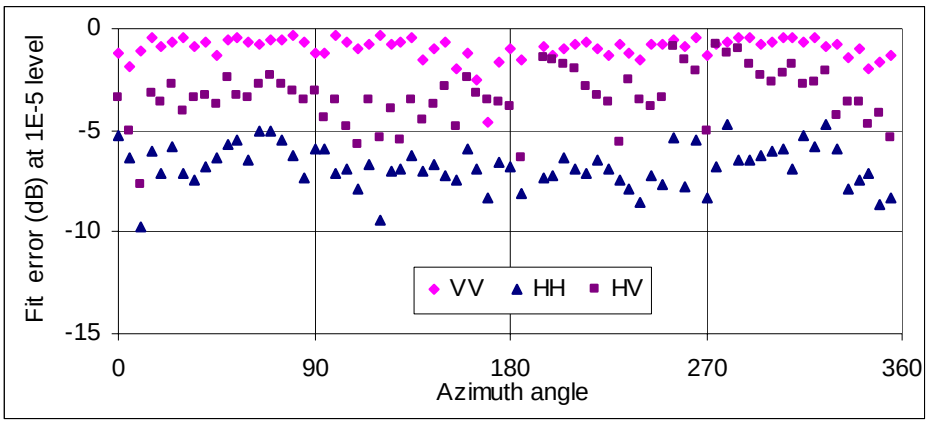


(a) Weibull fit

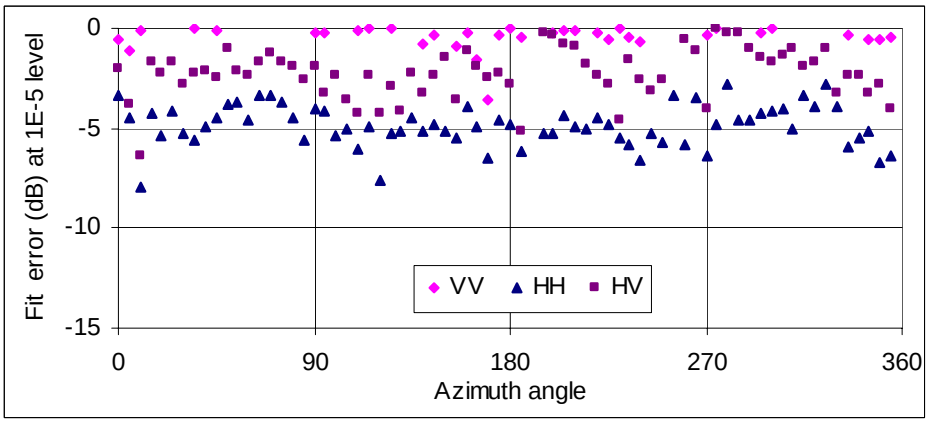


(b) K fit

*Figure 19: Difference in dB between the fitted cdf and the actual cdf at 1-cdf equal to $10^{-5}$ for datasets of run34690.*

# 5. KA Distribution

The phenomenon of the sudden departure of the sea clutter distribution from the K distribution in the tail region is believed to be attributed to sea spikes (Middleton, 1999, Watts et al, 2005). The finer the radar resolution, the more severe is the phenomenon. The understanding and modelling of such spikes are important for the prediction of radar performance and for guidance in developing improved target detection algorithms. Ward and Tough (2002), Watts et al (2005) use a KA distribution to improve the fit of the sea clutter distribution particularly in the tail region. The

character A simply means Class A (Middleton, 1999). In the KA distribution, the combination of Bragg and distributed whitecap scatterers is assumed to have a standard K distribution, and the discrete spikes (bursts and whitecaps confined in range extent) are assumed to be a Poisson distribution (Watts et al, 2005). In the presence of added noise, the overall distribution of amplitude $x$ is described using the compound formulation expressed as,

$$p(x\,|\,t)=\sum_{n=0}^{\infty}\frac{2x}{t+\sigma_n+n\sigma_{sp}}\exp\left(-\frac{x^2}{t+\sigma_n+n\sigma_{sp}}\right)p_{poisson}(n) \tag{34}$$

where $t$ is the local intensity of Bragg/whitecap scatterers which is gamma distributed as[7],

$$p(t)=\frac{1}{\Gamma(\nu)}t^{\nu-1}\left(\frac{\nu}{\sigma_{bw}}\right)^{\nu}\exp\left(-\frac{\nu t}{\sigma_{bw}}\right) \tag{35}$$

The Poisson distribution is given by,

$$p_{poisson}(n)=\exp(-\overline{N})\frac{\overline{N}^{n}}{n!} \tag{36}$$

where $\overline{N}$ is the mean number of spikes in each range cell, and $n$ the number of spikes in a given range cell. The overall clutter distribution is the integral of

$$p(x)=\int_0^{\infty}p(x\,|\,t)\,p(t)dt \tag{37}$$

The noise, spikes and Bragg/whitecap scatterers are assumed to be mutually uncorrelated, so that,

$$\sigma=E\{x^2\}=\sigma_n+\overline{N}\sigma_{sp}+\sigma_{bw} \tag{38}$$

where $\sigma$, $\sigma_n$, $\sigma_{sp}$ and $\sigma_{bw}$ are the mean clutter intensity, mean noise intensity, mean spike intensity and mean Bragg/whitecap intensity, respectively. If $\sigma_n=\sigma_{sp}=0$, $\overline{N}=0$ and letting $t=4y^2/\pi$ and noting $b^2=\frac{4}{\pi}\frac{\nu}{\sigma}$ the above KA distribution given by

[7] The local mean amplitude $y$ (with a scale factor) is used in (2). The relationship between $y$ in (2) and $t$ in (35) is $t=4y^2/\pi$.

(34)-(37) simplifies to the standard K distribution given by (2)-(3) as discussed in Section 2.

There are five parameters in a KA distribution, i.e., $\sigma_n$, $\sigma_{sp}$, $\sigma_{bw}$, $\overline{N}$ and $\nu$. Equation (38) defines one of their relationships, the noise intensity $\sigma_n$ is measurable, and we would need another three equations in order to determine all five parameters. Normally the method of moments offers such a possibility. In general however, it is difficult to determine all the parameters using the moment method since higher order moments may be difficult to obtain. Even if the relationships can be determined using moment methods, the parameter values derived might not be the ones we are expecting. For instance, using the 4th moment, Ward and Tough (2002) derive a formula to determine the shape parameter $\nu_{bw}$, for Bragg/whitecap scatterers, expressed as a function of the global shape parameter $\nu$ and other parameters including $\sigma_{sp}$, $\sigma_{bw}$, $\overline{N}$. We found, however, this sometimes even results in negative values of $\nu_{bw}$. Realising that the data distribution usually departs from the K distribution only in the region of $cdf > 0.999$, it is rational not to discriminate $\nu$ and $\nu_{bw}$, i.e., let $\nu_{bw} \approx \nu$ as assumed in (35). Therefore, the method of determining $\nu$ discussed in Section 2 remains unchanged. For a given radar system, its noise level $\sigma_n$ (or the clutter-to-noise ratio, $CNR = (\sigma_{bw} + \overline{N}\sigma_{sp})/\sigma_n$) can be determined. Finally, Watts et al (2005) and Ward and Tough (2002) suggest to set $\overline{N} = 0.01$, and $\rho = \sigma_{sp}/\sigma_{bw}$ in the range of 0 to 40 depending the strength of the spikes.

Figure 20 shows a comparison between a K distribution and a KA distribution. Parameters used in this example are $\nu = 3.5$, $\sigma = 0.1$, $\sigma_n = 0$, $\rho = 10$ and $\overline{N} = 0.01$. It can be seen in Figure 20 (b) that by adding the spike component, the KA distribution exhibits a sudden departure from the K distribution in the tail region, similar to the actual sea clutter distribution observed in the previous Section. It is therefore believed to be a better fit to sea clutter in the tail region for some situations. It is also noted from Figure 20 (a), however, that the KA distribution does not exactly agree with the K distribution in the low and mid regions.

The cdf comparison between the KA and K distributions are shown in Figure 21. Two KA cdfs shown in the figure correspond to $\rho = 5$ and $\rho = 10$, respectively, and the other parameters remain the same as those used in Figure 20. This example demonstrates that the degree of the sudden departure from the K distribution can be modelled by choosing different spike parameters.

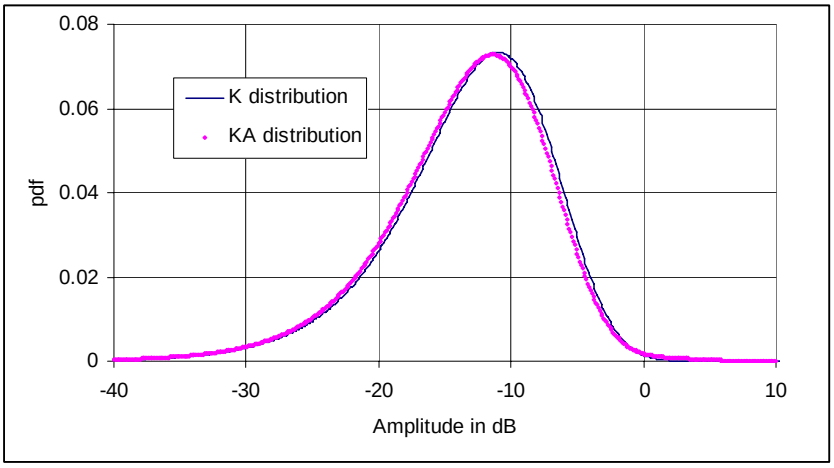


(a) pdf abscissa on linear scale to view global distribution

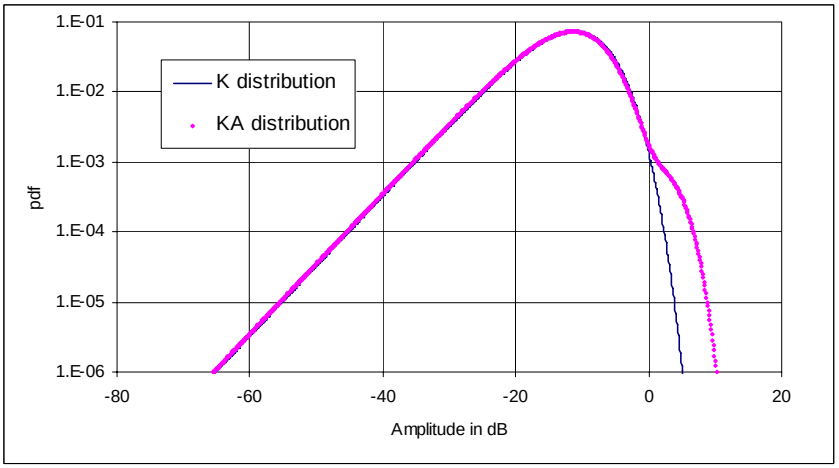


(b) pdf abscissa on log scale to view tail distribution

*Figure 20: Pdf omparison between KA and K distributions. Parameters used in the simulation are* $\nu = 3.5$, $\sigma = 0.1$, $\sigma_n = 0$, $\rho = 10$ *and* $\overline{N} = 0.01$.

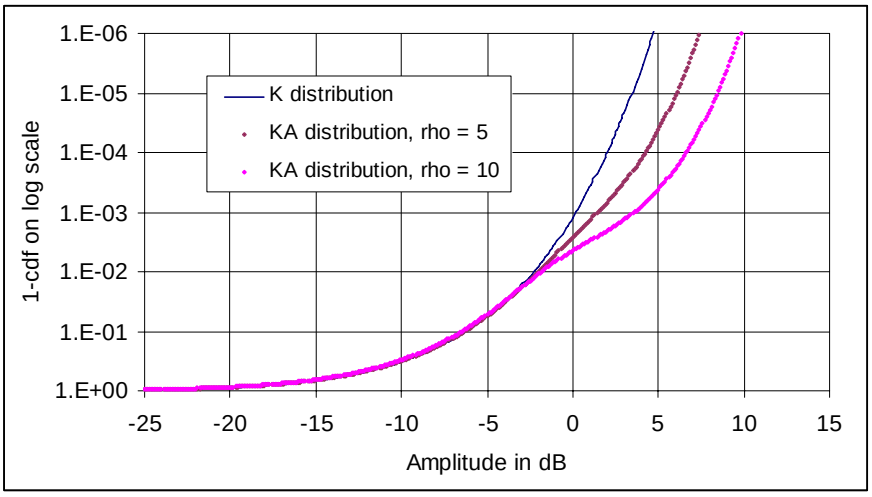


*Figure 21: Cdf comparison between the KA and K distributions. Two KA cdfs correspond to* $\rho = 5$ *and* $\rho = 10$ *, respectively, and the other parameters remain the same as those used in Figure 20.*

The fitted KA distribution for the HH polarised data of run34683_rccal_190 shown in Figure 15 is plotted in Figure 22 and Figure 23, together with the K distribution fit for comparison. It can be seen that the KA distribution significantly improves the fit in the tail region.

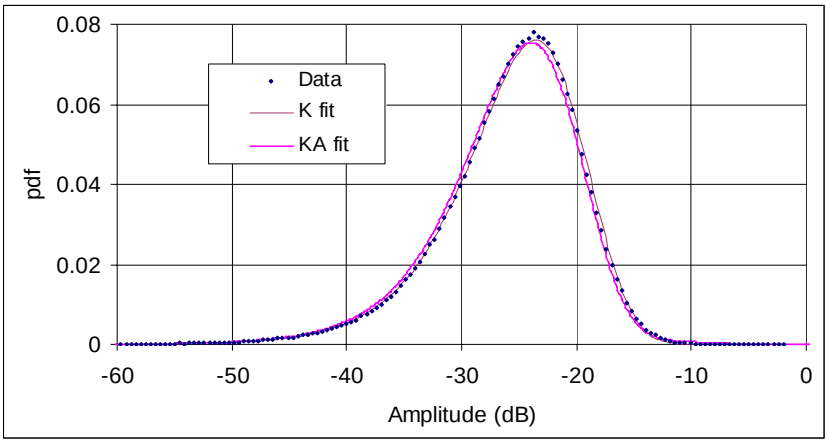


(a) pdf abscissa in linear scale to view global fit

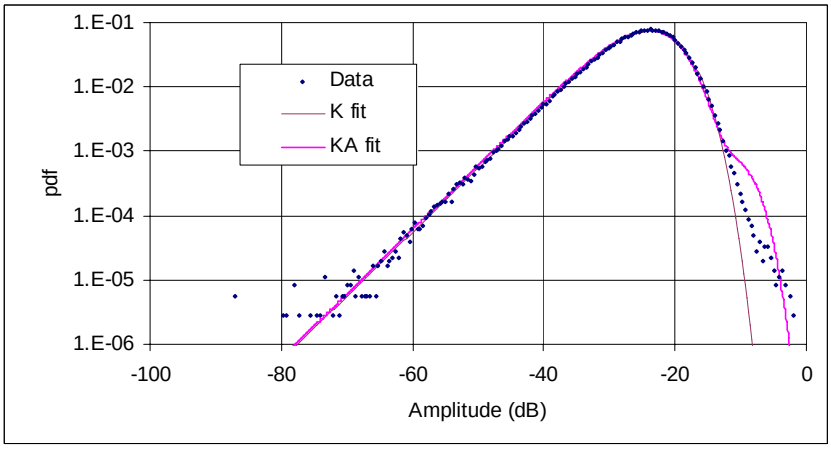


(b) pdf abscissa on log scale to view tail fit

*Figure 22: The distribution of the sea clutter dataset shown in Figure 15 is re-fitted with the KA distribution. Parameters used in the KA distribution are* $\sigma_n = 0$, $\rho = 10$ *and* $\overline{N} = 0.01$. *The previous K distribution fit is also shown for comparison.*

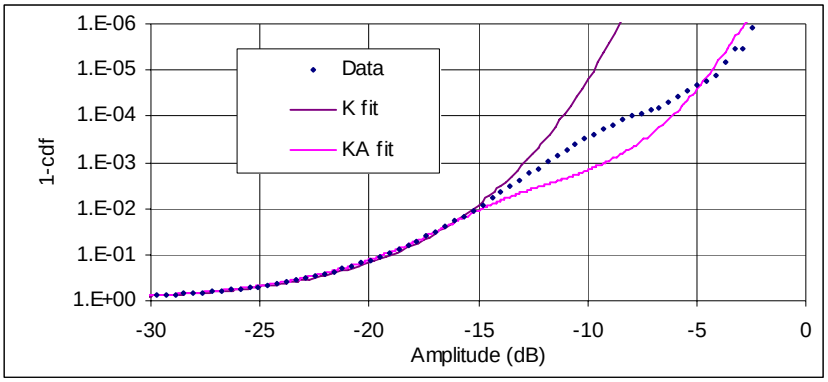


*Figure 23: Cdf comparison between the data distribution and the fitted KA distribution. The cdf of the previously fitted K distribution is also shown for comparison.*

Figure 16 and Figure 17 have demonstrated that the goodness of the classical K fit to sea clutter distribution varies, although the HH data generally contain more spikes than the other two polarised data. It therefore can be concluded that in general there are no universal parameters ($\overline{N}$ and $\rho$) of the spike component for the KA distribution. There is also no systematic way to estimate $\overline{N}$ and $\rho$ parameters, and the estimation involves a 'try and see' process.

Apart from the problem that not all parameters of a KA distribution can be determined solely from a given dataset, the other problem of the KA distribution is that the distribution cannot be expressed in closed form. Therefore, the pdf and cdf of a KA distribution can only be numerically computed using (34)-(37).

# 6. KK Distribution

## 6.1 KK distribution

The KA distribution significantly improves the agreement of the fitted distribution and the sea clutter distribution in the tail region, if the spike component exists. It may also physically explain why the distribution of spiky sea clutter departs from the classical K distribution in the tail region. Its main drawback however is that the distribution cannot be expressed in closed form, and its pdf and cdf have to be numerically computed, which is computationally expensive. It therefore significantly increases the difficulty for the analysis of radar performance and for the derivation of the threshold multiplier usually required by the target detection process, such as CFAR algorithms.

In this Section we introduce a KK distribution for sea clutter distribution fit if the spike component exists. The KK distribution assumes that both the Bragg/whitecap scatterers and spikes are K-distributed, and the overall clutter distribution is the mixture of the two K distributions, as,

$$p(x) = (1-k)\,p_1(x;\nu,\sigma) + k\,p_2(x;\nu_{sp},\sigma_{sp}) \tag{39}$$

where $p_1$ and $p_2$ are K-distributed functions with the specified shape parameter and the mean intensity (note, $\sigma = 4\nu/c^2$ as given in Table 1) in the brackets. If $k = 0$, $p(x) = p_1(x;\nu,\sigma)$ and it simplifies to the usual K distribution without the spike component. Since the sea clutter distribution usually departs from the K distribution at 1-cdf equal to about $10^{-3}$ or higher, it is rational to assume the shape parameter and the mean intensity of Bragg/whitecap scatterers in $p_1(x;\nu,\sigma)$ are the same as the K parameters discussed in Section 2. The selection of $k$, $\nu_{sp}$ and $\rho = \sigma_{sp}/\sigma$ together determines the spike component[8]. It is found empirically that the shape parameter of $p_2(x;\nu_{sp},\sigma_{sp})$ can be set to the same value of $p_1(x;\nu,\sigma)$, i.e., $\nu_{sp} = \nu$. The selection of $\rho$ mainly determines the degree of the separation between two distributions in the tail region while the selection of $k$ affects both the departure level and the degree of the separation.

Figure 24 compares the K, KA and KK distributions for the example shown in Figure 20. The selection of the parameters for the KK distribution is $\nu_{sp} = \nu$, $\rho = \sigma_{sp}/\sigma = 7$ and $k = 0.01$. It can be seen from Figure 24 (b) that the KK distribution is nearly identical to the KA distribution in the tail region. On the other hand, as shown in Figure 24 (a), the global discrepancies between the KK and K distributions are unnoticeable, whereas the existence of the global discrepancies between the KA and K distributions is obvious.

[8] In the KA distribution $\rho = \sigma_{sp}/\sigma_{bw}$ differs from the definition in the KK distribution.

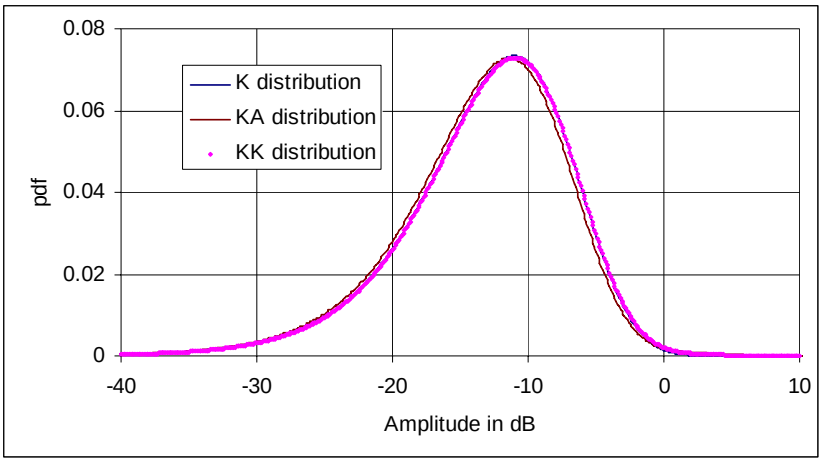


(a) pdf abscissa on linear scale to view global distribution

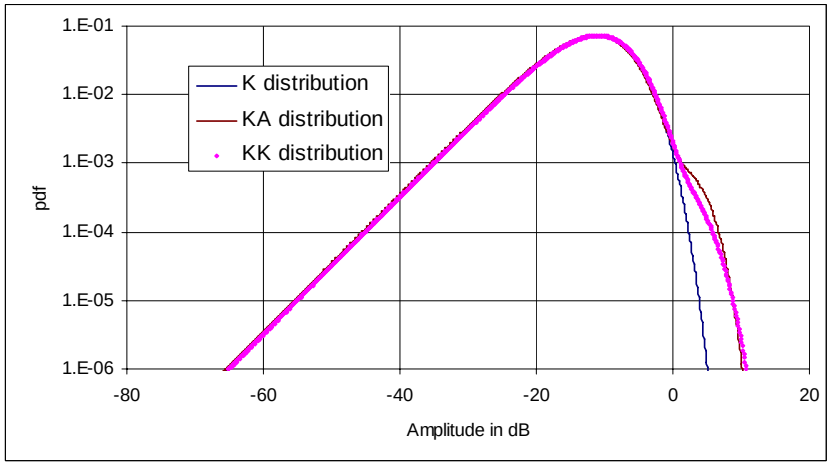


(b) pdf abscissa on log scale to view tail distribution

*Figure 24: Comparison between K, KA and KK distributions. Parameters for the K and KA distributions are the same as those used in Figure 20. Parameters for the KK distribution are* $\nu_{sp} = \nu$, $\rho = \sigma_{sp}/\sigma = 7$ *and* $k = 0.01$. *The K and KK distributions totally appear coincident in plot (a).*

The cdf comparison between these three distributions is shown in Figure 25. It can be seen that the cdfs of the KK and KA distributions are very close in the tail region.

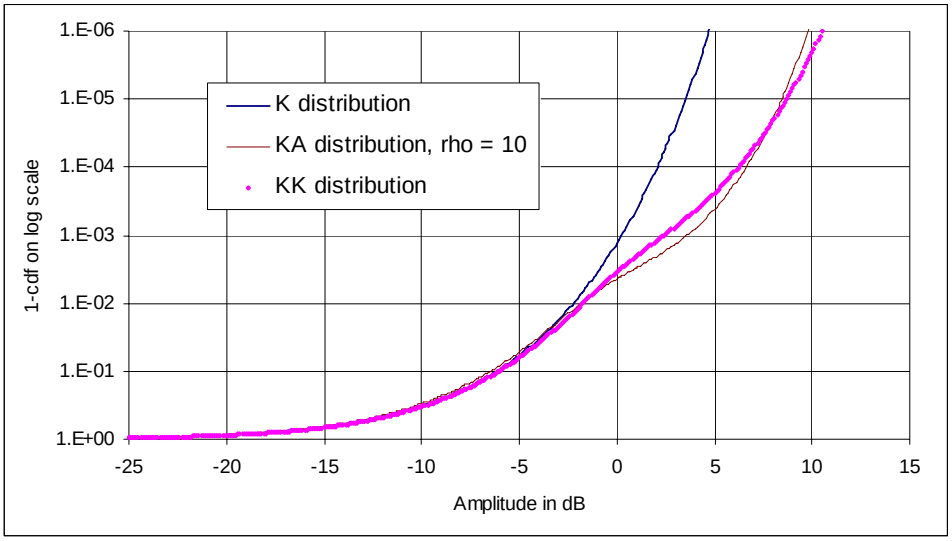


*Figure 25: Cdfs of the K, KA and KK distributions for the example shown in Figure 24. The cdfs of the KA and KK distributions are very close in the tail region.*

The influence of the parameters $k$ and $\rho$ over the KK distribution in the tail region is demonstrated in Figure 26. It can be seen that the parameter $\rho$ mainly influences the degree of the separation between the K and KK distributions while the parameter $k$ affects both the departure level and the separation.

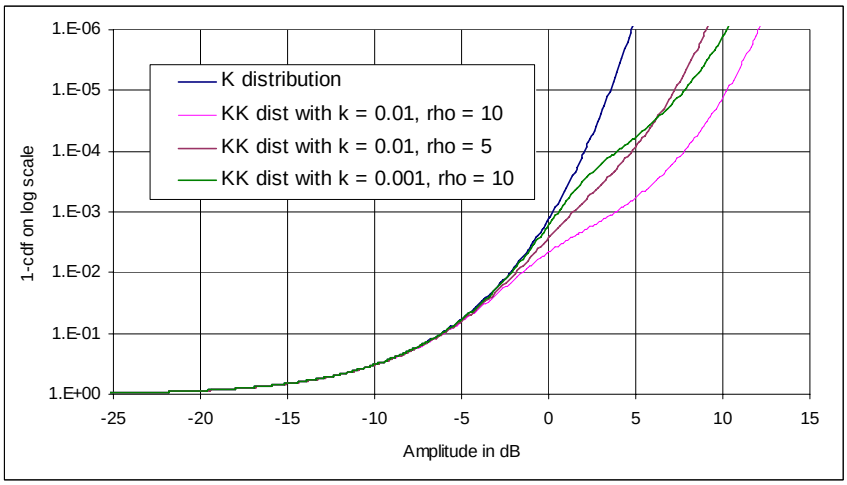


*Figure 26: KK distribution with different spike parameters. It is shown that the parameter $\rho$ mainly influences the degree of the separation between the K and KK distributions while the parameter $k$ affects both the departure level and the separation.*

The data fit shown in Figure 22 and Figure 23 is replotted and shown in Figure 27 and Figure 28. The KK fit is plotted together with the KA and K fits for comparison. It is seen that the fit of the proposed KK distribution is better than the KA distribution not only in the tail region (refer to Figure 27 (b) and Figure 28) but also in other regions (refer to Figure 27 (a)) for the parameters used.

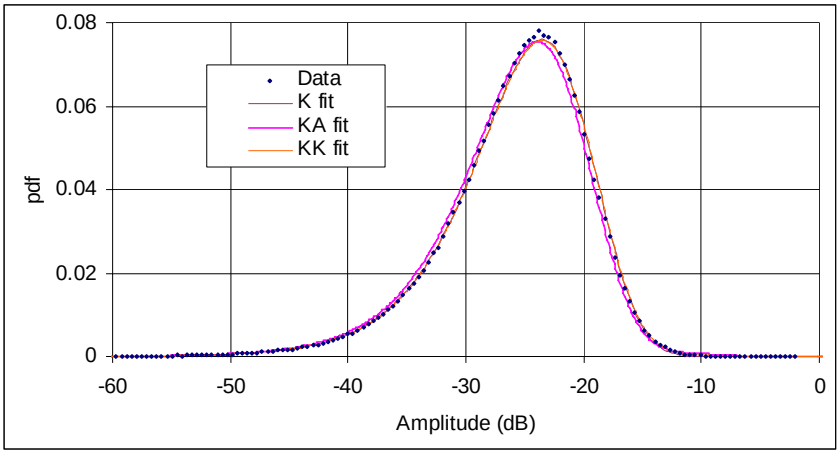


(a) pdf abscissa in linear scale to view global fit

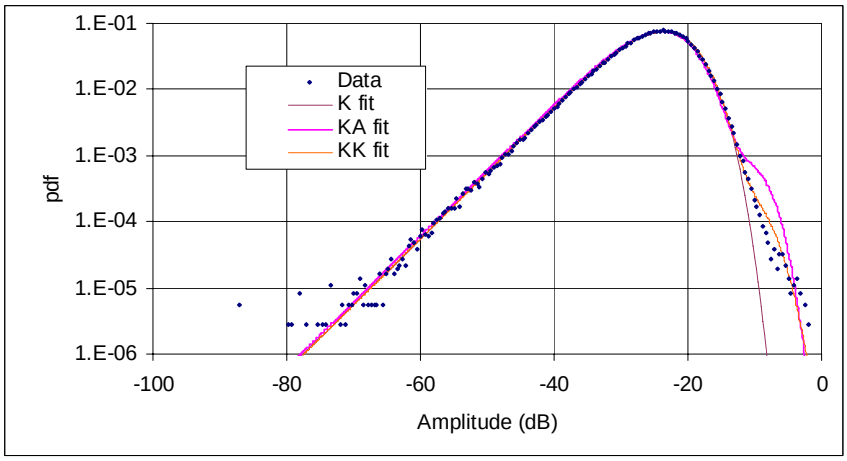


(b) pdf abscissa on log scale to view tail fit

*Figure 27: The distribution of the sea clutter dataset shown in Figure 22 is replotted. The KK fit is also shown. The KK parameters used are* $k = 0.005$ *and* $\rho = 8$.

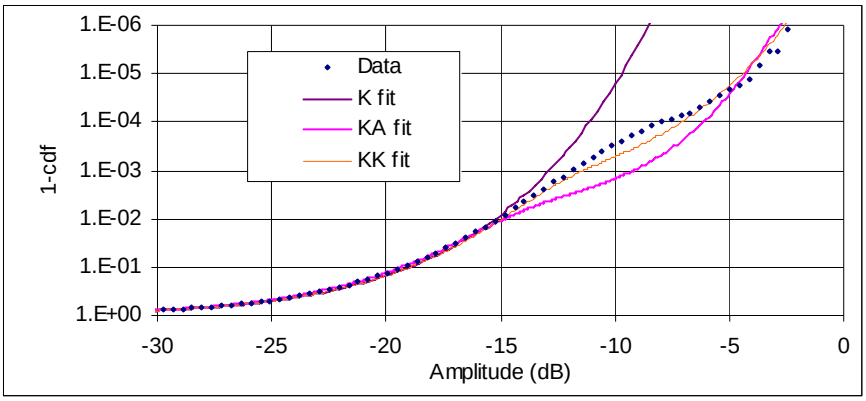


*Figure 28: Cdf comparison between the data distribution and the fitted KA and KK distributions. The cdf of the fitted K distribution is also shown for comparison.*

## 6.2 Discrepancies between Data and Fitted KK Distributions

It has been shown in Section 4 that in the region beyond cdf > 0.999, some datasets can be fitted well by either K or Weibull distributions, and others cannot. In this Subsection, we use the KK distribution to improve the fit for the tail region. To simplify the algorithm, we first tabulate the cdf separation, between the K and KK distributions, as a function of $\rho$ with the fixed values of $k = 0.01$ and $\nu = 4.75$ ($\nu = 4.75$ is the median value for datasets of run34690 and run34683), which is shown in Figure 29. Obviously if we use the true value of $\nu$ to create the lookup table for each dataset, the results might be better but at a higher cost of computation.

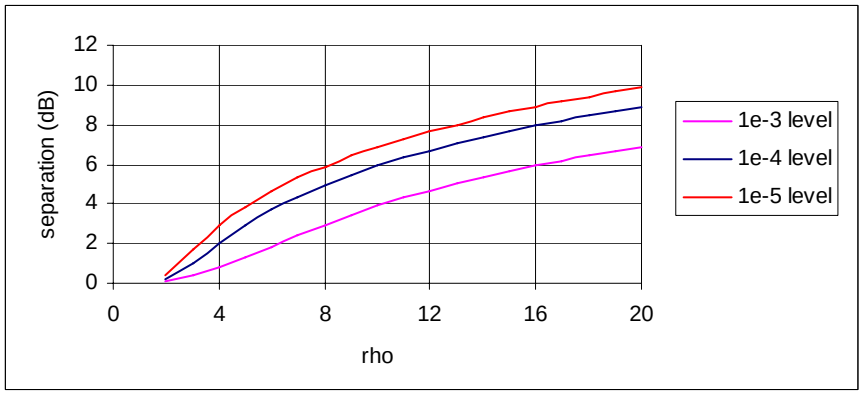


*Figure 29: Cdf separations between the K and KK distributions as a function of $\rho$ at the levels of 1-cdf equal to $10^{-3}$, $10^{-4}$ and $10^{-5}$, respectively. The selection of other two parameters is $k = 0.01$, and $\nu = 4.75$.*

Using the lookup table as shown in Figure 29, our KK fit process involves the following steps:

1. Find the shape parameter and scale parameter for the K distribution;
2. Compute the 1-cdf differences between the fitted K and data distributions at $10^{-3}$, $10^{-4}$ and $10^{-5}$;
3. Find $\rho$ values corresponding to the computed 1-cdf differences from the lookup table of Figure 29;
4. Use the mean of $\rho$ and $k = 0.01$ as the final values for the KK fit.

Discrepancies of the KK fit for datasets of run34683 and run34690 at 1-cdf equal to $10^{-3}$ and $10^{-5}$ are shown in Figure 30 and Figure 31, respectively. It can be seen that the KK distribution significantly improves the fit in the tail region. Compared to Figure 17 and Figure 19, where the typical cdf difference between the K and data distributions was around $-4$ to $-5$dB at the $10^{-5}$ level for the HH data, this difference now reduces to around ±1dB.

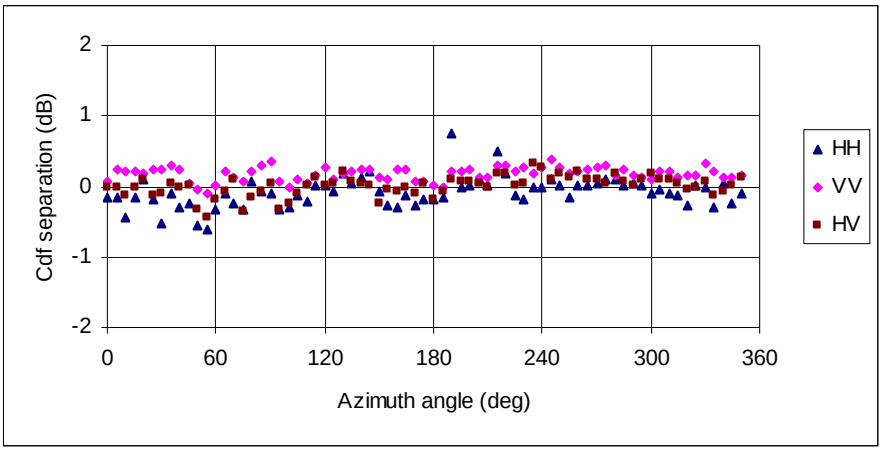


(a) run34683

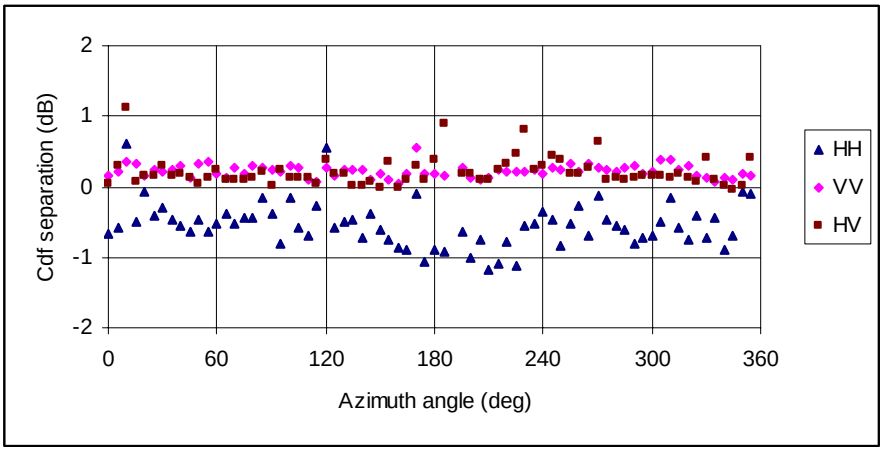


(b) run34690

*Figure 30: Difference in dB between the fitted KK cdf and the actual cdf at the $10^{-3}$ level for datasets run34683 and run34690.*

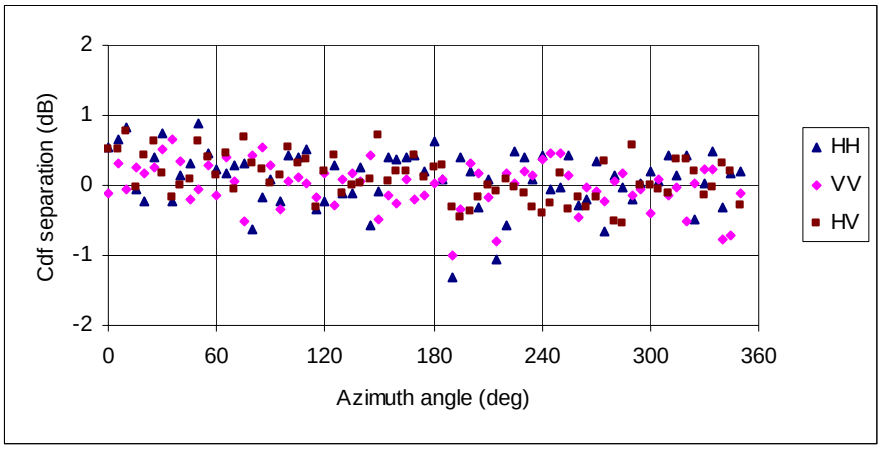


(a) run34683

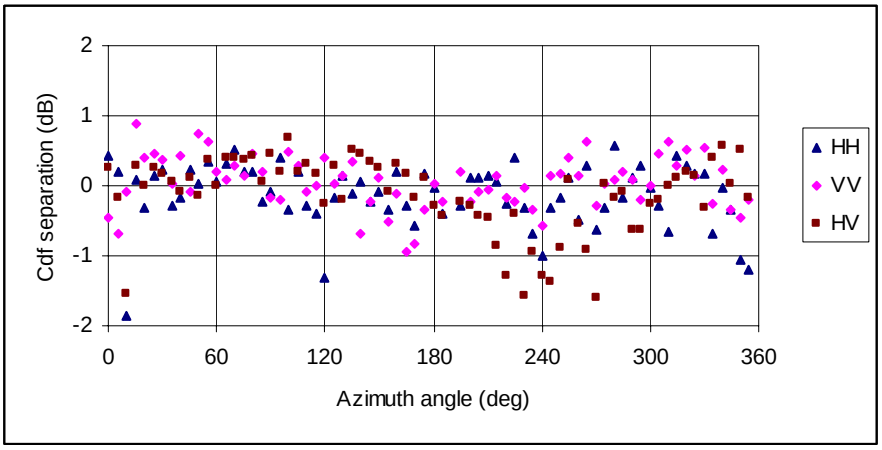


(b) run34690

*Figure 31: Difference in dB between the fitted KK cdf and the actual cdf at the $10^{-5}$ level for datasets run34683 and run34690.*

Values of the parameter $\rho$ used for the KK fit are shown in Figure 32. It is seen that the distribution of the VV data can almost be fitted with the K distribution (when $\rho = 1$ the KK distribution simplifies to the K distribution). The HH data is spikiest, and the typical values of $\rho$ are about 4 for run34683 and 7 for run34690. We also see that overall the fit for the datasets of run34683 is better than that of for the datasets of run34690. Whether this is due to the incidence angle is unclear at this stage.

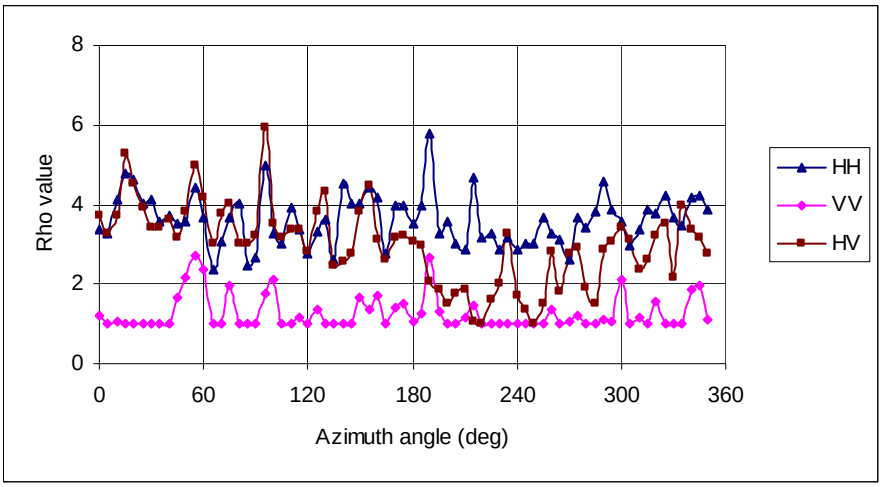


(a) run34683

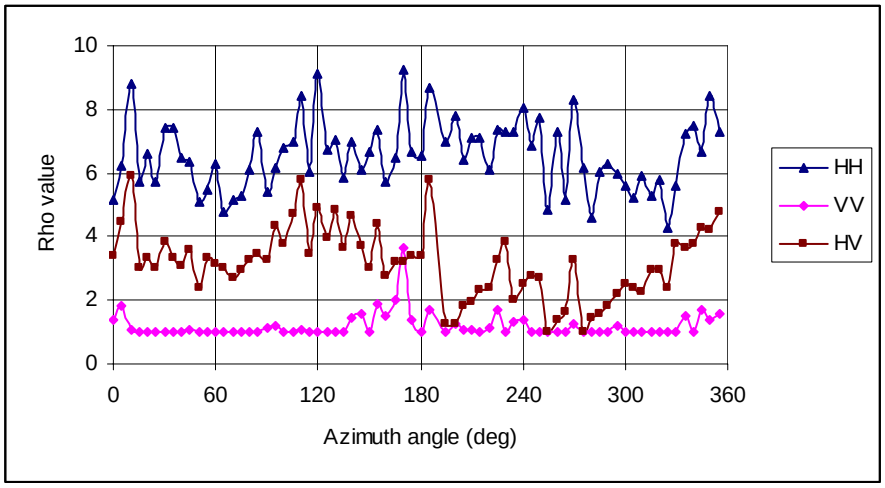


(b) run34690

*Figure 32: The value of $\rho$ used in the KK fit. The parameter $k = 0.01$ is fixed for all datasets.*

# 7. Weibull-Weibull Distribution

## 7.1 WW Distribution

The fact that the Weibull distribution is very similar to the K distribution naturally leads to considering using a Weibull-Weibull (WW) distribution to fit sea clutter with spikes. Similar to the KK distribution, the WW distribution can be defined as,

$$p(x) = (1-k)\, p_1(x;b,\sigma) + k\; p_2(x;b_{sp},\sigma_{sp}) \tag{40}$$

where $p_1(x;b,\sigma)$ and $p_2(x;b_{sp},\sigma_{sp})$ represent the distribution of Bragg/whitecap scatterers and spikes, respectively. Similar to the explanations given for the KK distribution, the parameters $b$ and $\sigma$ of $p_1(x;b,\sigma)$ can be considered to be equal to the global $b$ and $\sigma$ of the data. As given in Table 2, the mean intensity $\sigma$ is a function of $b$ and $c$, as, $\sigma = \Gamma(1+2/b)/c^{2/b}$. The shape parameter $b_{sp}$ for the spike component can be assumed to be equal to the global shape parameter, i.e., $b_{sp} = b$. The free parameters, $k$ and $\rho = \sigma_{sp}/\sigma$ determine the component of spikes. If $k = 0$ or $\rho = 1$, the WW distribution simplifies to the Weibull distribution.

The HH data of run24683_rccal_190, discussed before, is fitted using the WW distribution with $k = 0.01$ and $\rho = 9$, and the results are shown in Figure 33 and Figure 34. The previous K and KA results are also shown for comparison. It is seen that in the tail region the WW distribution is nearly identical to the KA distribution. The global agreement between the data distribution and the WW distribution, as shown in Figure 33 (a), however is not as good as that of the K distribution, which can also be observed from Figure 15 (a).

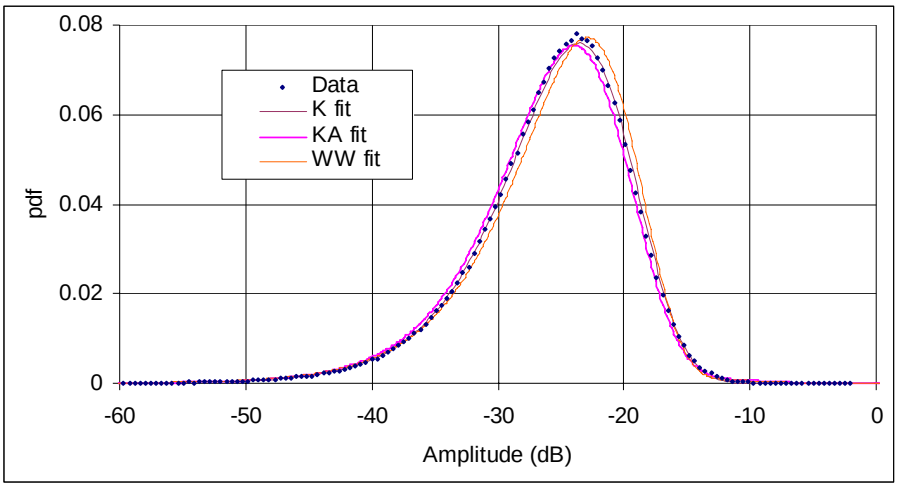


(a) pdf on linear scale to view global fit

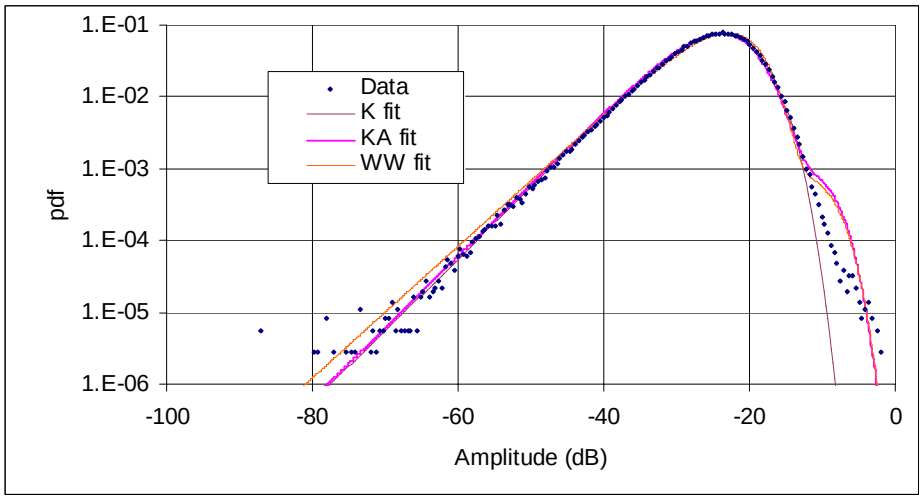


(b) pdf on log scale to view tail fit

*Figure 33: The WW fit to the distribution of sea clutter with spikes. The K and KA fits are also shown for comparisons. The WW parameters used are* $k = 0.01$ *and* $\rho = 9$.

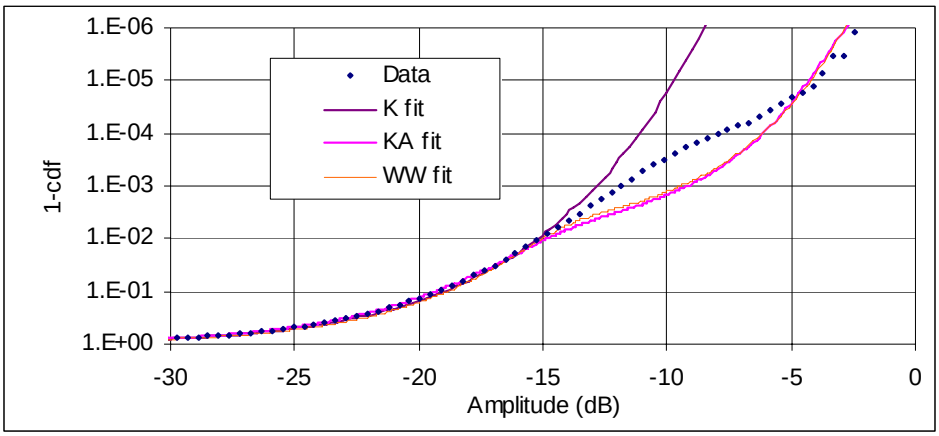


*Figure 34: Cdf comparison between the data, K, KA and WW distributions.*

## 7.2 Discrepancies between Data and Fitted WW Distributions

The similar method for determining the KK parameters is used for the determination of the WW parameters. We first tabularise the cdf separation as a function of $\rho$ for the given parameters of $k = 0.01$ and $b = 1.8$ (the median value of the datasets) at the levels of 1-cdf equal to $10^{-3}$, $10^{-4}$ and $10^{-5}$, respectively, as shown in Figure 35.

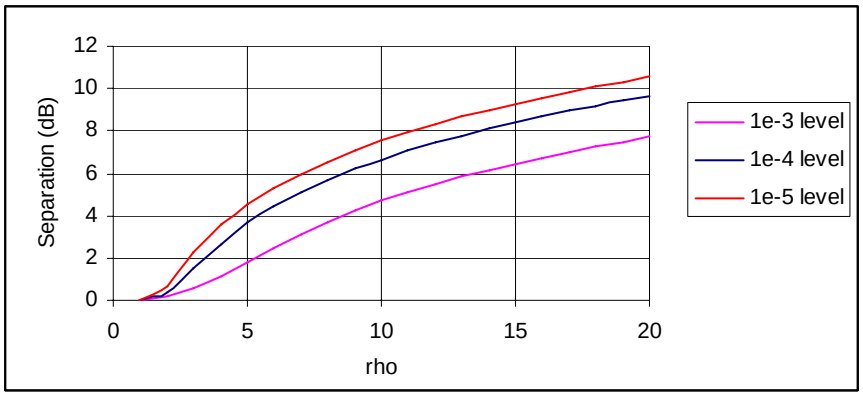


*Figure 35: The cdf separations between the Weibull and WW distributions as a function of $\rho$ at the levels of 1-cdf equal to $10^{-3}$, $10^{-4}$ and $10^{-5}$, respectively, with the given parameters $k = 0.01$ and $b = 1.8$.*

The WW fit process involves the following steps.

1. Find the shape and scale parameters for the Weibull distribution;
2. Compute the cdf differences between the data and the fitted Weibull distributions at 1-cdf equal to $10^{-3}$, $10^{-4}$ and $10^{-5}$;
3. Find $\rho$ values corresponding to the cdf differences from the lookup table of Figure 35;
4. Use the mean of $\rho$ and $k = 0.01$ as the final parameters for the WW fit.

Discrepancies between the WW fit and datasets for run34683 and run34690 at 1-cdf equal to $10^{-3}$ and $10^{-5}$ are shown in Figure 36 and Figure 38. Compared to the results of the Weibull fit shown in Figure 17 and Figure 18, it can be seen that the WW fit significantly improves the fit in the tail region. For instance, the cdf separation for the run34690 HH data at the $10^{-5}$ level is about −7dB if Weibull fit is used, this figure is reduced to and confined in about ±1dB should the WW fit be applied. Overall the fit of the WW distribution in the tail region is almost as good as that of the KK distribution.

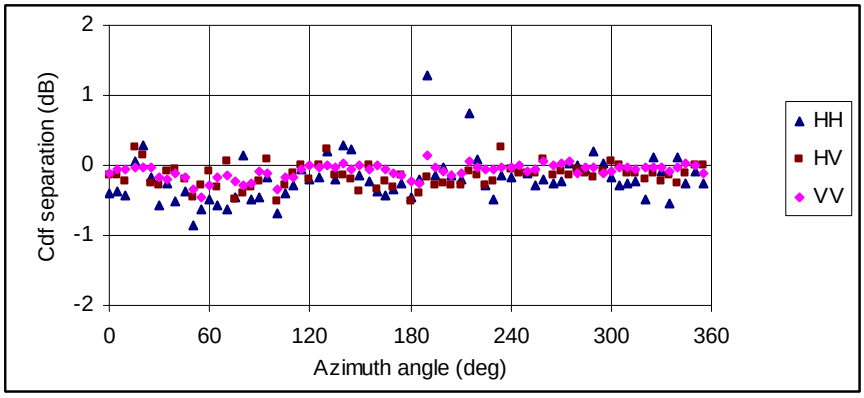


(a) run34683

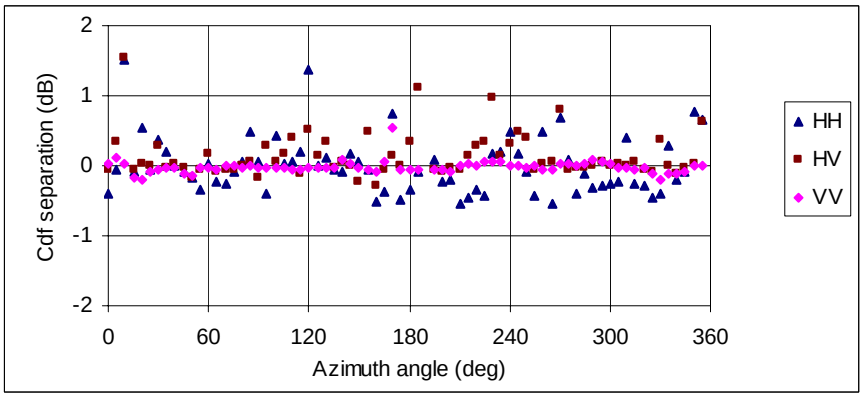


(b) run34690

*Figure 36: Difference in dB between the fitted WW cdf and the actual cdf at the 1-cdf equal to $10^{-3}$ for datasets run34683 and run34690.*

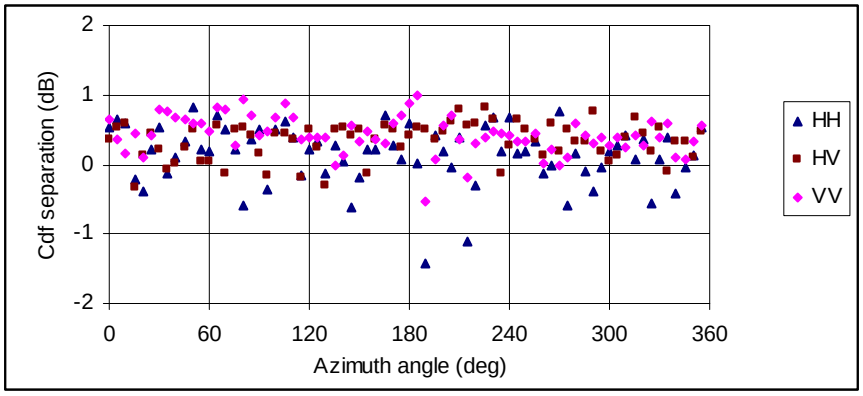


(a) run34683

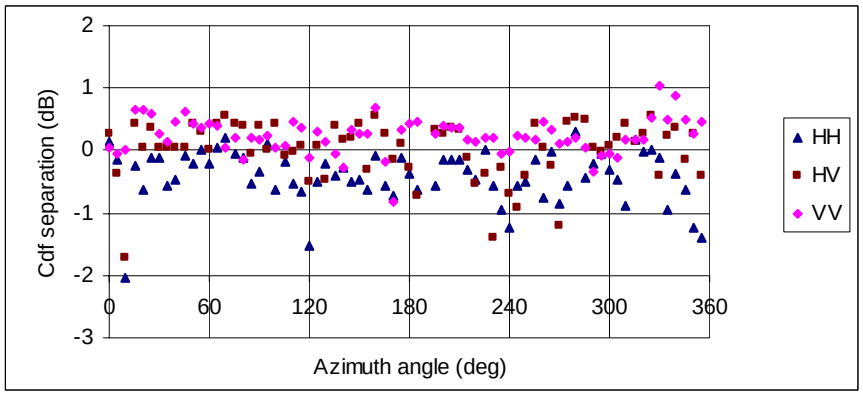


(b) run34690

*Figure 37: Difference in dB between the fitted WW cdf and the actual cdf at 1-cdf equal to $10^{-5}$ for datasets run34683 and run34690.*

Figure 38 shows the parameter $\rho$ used in the WW fit process. Since the Weibull distribution normally converges a little faster than the K distribution, the $\rho$ values are generally bigger than the values used in the KK fit to slow down the convergence. For the VV data, the $\rho$ values for the KK fit are around 1, indicating the traditional K distribution is a good fit. In the case of the WW fit for the VV data, however, the $\rho$ values are around 2, indicating the traditional Weibull distribution is conservative and needs to be compensated by choosing $\rho > 1$ in order to fit the data distribution in the tail region. Since the WW distribution can alter its convergence by choosing different $\rho$ values, it is therefore possible to tune its convergence to be as good as that of the KK distribution.

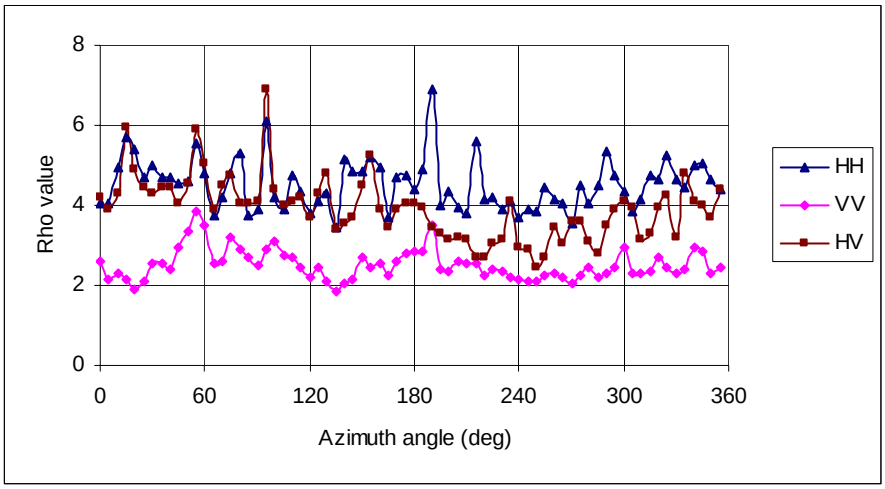


(a) run34683

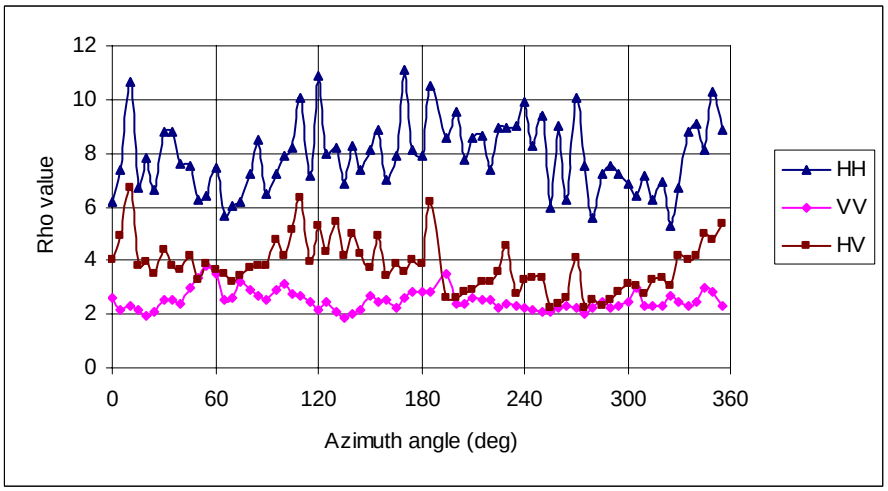


(b) run34690

*Figure 38: The value of $\rho$ used in the WW fit. The parameter $k = 0.01$ is fixed for all datasets.*

# 8. Conclusions

Distribution of X-band, high range resolution (0.75m) and high incidence angle ($50^o$ and $70^o$) sea clutter data, collected by the DSTO developed airborne radar system, Ingara, in the Sea Clutter Trial 2004, has been studied. Each dataset used in the analysis consists of about $10^6$ samples, corresponding to a span of $3.5^o$ to $8^o$ in incidence angle

change (depending on nominal incidence angle), and a span of $5^o$ in azimuth angle change. Since the incidence angle is in the plateau region (Long, 2001) and the span of the azimuth angle is narrow, we can consider the distribution studied to be the same as the spatial distribution. The size of the samples provides a reliable distribution up to 1-cdf equal to the $10^{-5}$ level.

The mean clutter varies periodically in azimuth with the maxima and the minima in the upwind and crosswind directions, respectively, and the second peak corresponding to the downwind direction. The shape parameter of clutter distributions, however, does not show a noticeable azimuthal pattern correlated with wave/wind directions.

It has been found that the VV data has the lowest spiky level compared to the HH and HV data. In general the VV data can be fitted by a K distribution with the shape parameter varying from about 4 to 25.

The HH data is spikiest and its distribution exhibits a sudden departure from the K distribution in the tail region, often in the region of 1-cdf equal to $10^{-3}$ and beyond due to discrete sea spikes. To tackle this problem, the KA, KK and WW distributions (the latter two have been first proposed in this report) have been used to improve the agreement between the data and fitted distributions in the tail region. It has been shown that the difference, which can be as large as about −7dB between the data cdf and the K cdf at the 1-cdf equal to $10^{-5}$ level, can be reduced to about ±1dB if the KK distribution is used to model the data distribution.

The KA distribution cannot be expressed in closed form, and it is computationally very expensive. It also imposes a difficulty to the analysis of radar performance, as the analysis often involves the clutter distribution function. Aimed at simplifying the distribution function, this report has proposed a KK distribution, which is a mixture of two K distributions of which one representing the distribution of Bragg/whitecap scatterers and the other for the distribution of sea spikes. We have shown that the KK distribution is as good as the KA distribution in terms of agreement in the tail region. In addition, the KK distribution introduces the least distortion to the K distribution in the low and mid regions. Mathematically, a KK distribution is simply a mixture of two K distributions.

Since the Weibull distribution is very close to the K distribution, this report has also proposed a WW distribution to improve the agreement between the data pdf and the fitted pdf in the tail region. A WW distribution is a sum of two Weibull distributions. In general, a Weibull distribution converges a little faster than a K distribution for shape parameters normally found in sea clutter statistics, which often leads to a bigger discrepancy between the data pdf and the Weibull pdf in the tail region. The Weibull fit, even for the VV data is not as good as the K fit. This however can be compensated if a WW distribution is used, as the convergence of the WW distribution is tuneable. The

results show that the fit of the WW distribution in the tail region is comparable to the KK or KA distribution. However, in the low and mid region, the agreement between the data pdf and the WW pdf is not as good as that between the data pdf and KK pdf.

The report has also proven that a Weibull distribution can be transformed to a Rayleigh or gamma distribution and vice versa through a non-linear but simple mapping. Therefore, in the case where clutter data is modelled as a Weibull distribution, the data may be first transformed accordingly and then treated as a Rayleigh or gamma distribution, as the Rayleigh or gamma distribution is much easier to deal with. For simulation, a Weibull distributed dataset can be easily generated from a transform of a Rayleigh distributed dataset.

CFAR schemes often employ local statistics of clutter to adaptively set the threshold for target detection. This report has also discussed the distribution of the sum of K or Weibull distributed samples. An approximate formula in closed form approaching the distribution of the sum of Weibull distributed samples has been proposed. Its accuracy has been numerically verified using both the convolution method and simulated data. No noticeable error between the proposed formula and the numerically evaluated values from the convolution method or simulated data has been found.

This report contributes to the delivery of *Milestone 4.1.1.1.1: High grazing angle sea clutter and target signatures* in the AIR 7000 S&T Plan (Annex C – Technical Support Plan). The outcomes of the analysis contained herein will also form a component of the model delivered for *Milestone 4.1.1.1.2: Radar modelling capability development – maritime* of the Technical Support Plan. These activities are aimed at better understanding of the radar performance drivers for operation of High Altitude Long Endurance (HALE) UAVs in the maritime surveillance role, and therefore reducing risk in any acquisition decision.

# 9. Acknowledgement

ISRD of DSTO provided the sea clutter data for this study. In particular, the support from Mr R Smith and Mr M Preiss, and discussions with Dr D Crisp are acknowledged. Comments made by Dr B Haywood and Dr A Shaw improved the readability.

# 10. References

Anastassopoulos, V, and Lampropoulos, G A, "Optimal CFAR detection in Weibull clutter", IEEE Trans on Aerospace and Electronic Systems, vol. 31, no.1, pp. 52-64, 1995.

Antipov, I, "Analysis of sea clutter data", Technical Report, DSTO-TR-0647, Defence Science Technology Organisation, Australia, 1998.

Armstrong, B C, and Griffiths, H D, "CFAR detection of fluctuating targets in spatially correlated K-distributed clutter", IEE Proc Radar, Sonar and Navigation, vol. 138, no. 2, pp. 139-152, 1991.

Billingsley, J B, Low-Angle Land Clutter Measurements and Empirical Models, William Andrew Publishing, 2002.

Blacknell, D, "Comparison of parameter estimators for K distribution," IEE Proc Radar, Sonar and Navigation, vol. 141, no. 1, pp. 45-52, 1994.

Blacknell, D, and Tough, R J A, "Parameter estimation for the K-distribution based on [zlog(z)]", IEE Proc Radar, Sonar and Navigation, vol. 148, no. 6, pp. 309-312, 2001.

Crisp, D J, Stacy, N J S, and Goh, A S, "Ingara medium-high incidence angle polarimetric sea clutter measurements and analysis", Technical Report, DSTO-TR-1818, Defence Science Technology Organisation, 2006.

Dong Y, "Clutter spatial distribution and new approaches of parameter estimation for Weibull and K distributions", Research Report, DSTO-RR-0274, Defence Science Technology Organisation, Australia, 2004.

Jao, J K, "Amplitude distribution of composite terrain radar clutter and the K distribution," IEEE Trans on Antennas and Propagation, vol. AP-32, no. 10, pp. 1049-1062, 1984.

Levanon, N, and Shor, M, "Order statistics CFAR for Weibull background", IEE Proc Radar, Sonar and Navigation, vol. 137, no. 3, pp. 157-162, 1990.

Long, M W, Radar Reflectivity of Land and Sea, 3rd Edition, Artech House, 2001.

Middleton, D, "New physical-statistical methods and models for clutter and reverberation: The KA-distribution and related probability structures", IEEE Journal of Oceanic Engineering, vol. 24, no. 3, pp. 261-284, 1999.

Oliver, C J, "Optimum texture estimators for SAR clutter", Journal of Physics D: Applied Sciences, vol. 26, pp. 1824-1835, 1993.

Redding, N J, "Estimating the parameters of the K distribution in the intensity domain", Technical Report, DSTO-TR-0839, DSTO, 1999.

Sekine, M, and Mao, Y, Weibull Radar Clutter, Peter Peregrinus Ltd., 1990.

Skolnik, M I, Introduction to Radar Systems, 3rd Edition, McGraw-Hill, 2001.

Ulaby, F T, Moore, R K, and Fung, A K, Microwave Remote Sensing Active and Passive Volume II: Radar Remote Sensing and Surface Scattering and Emission Theory, Artech House, 1982.

Ward, K D, Baker, C J, and Watts, S, "Maritime surveillance radar Part I: Radar scattering from the ocean surface," IEE Proceedings, Pt F, vol. 137, no. 2, pp. 51-62, 1990.

Ward, K D, and Tough, R J A, "Radar detection performance in sea clutter with discrete spikes", International Radar Conference 2002, pp. 253-257.

Watts, S, "Radar detection prediction in sea clutter using the compound K distribution model," IEE Proceedings, Pt F, vol 32, no. 7, pp. 613-620, 1985.

Watts, S, "Radar detection prediction in K- distributed sea clutter and thermal noise," IEEE Trans on Aerospace and Electronic Systems, vol. AES-23, no. 1, pp. 40-45, 1987.

Watts, S, "Radar detection statistics in spatially correlated sea clutter", Statistical Signal Processing, IEE Colloquium on 6 Jan 1999.

Watts, S, Ward, K D, and Tough, R J A, "The physics and modelling of discrete spikes in radar sea clutter", Proceedings of International Radar conference, 2005.

Wilks, S S, Mathematical Statistics, John Wiley & Sons, 1962.

# Appendix A:

*Table A-1: Mean and shape parameters estimated for run34683 (incidence angle of 51.3°).*

| Azimuth angle (°) | Mean amplitude in dB | | | K shape parameter $\nu$ | | | Weibull shape parameter $b$ | | |
|---|---|---|---|---|---|---|---|---|---|
| | HH | VV | HV | HH | VV | HV | HH | VV | HV |
| 0 | -26.84 | -21.31 | -35.11 | 5.635 | 9.861 | 7.081 | 1.861 | 1.919 | 1.889 |
| 5 | -26.85 | -20.98 | -35.25 | 5.379 | 10.988 | 6.937 | 1.855 | 1.927 | 1.886 |
| 10 | -26.44 | -20.38 | -35.08 | 3.986 | 10.566 | 6.258 | 1.807 | 1.925 | 1.875 |
| 15 | -25.99 | -19.74 | -34.80 | 3.985 | 12.966 | 5.766 | 1.807 | 1.938 | 1.864 |
| 20 | -25.87 | -19.28 | -34.62 | 5.319 | 17.564 | 7.949 | 1.853 | 1.954 | 1.900 |
| 25 | -25.56 | -18.95 | -34.48 | 5.349 | 12.590 | 6.324 | 1.854 | 1.936 | 1.876 |
| 30 | -25.18 | -18.61 | -34.13 | 3.494 | 6.098 | 4.312 | 1.782 | 1.871 | 1.821 |
| 35 | -24.96 | -18.29 | -34.13 | 3.185 | 5.498 | 4.211 | 1.762 | 1.858 | 1.817 |
| 40 | -24.61 | -18.05 | -33.97 | 3.328 | 8.210 | 4.853 | 1.772 | 1.904 | 1.840 |
| 45 | -24.69 | -18.07 | -34.35 | 3.331 | 6.994 | 4.788 | 1.772 | 1.887 | 1.838 |
| 50 | -24.45 | -17.94 | -34.25 | 2.742 | 4.755 | 4.520 | 1.727 | 1.837 | 1.829 |
| 55 | -24.03 | -17.65 | -33.97 | 2.475 | 3.932 | 3.831 | 1.701 | 1.805 | 1.800 |
| 60 | -23.92 | -17.56 | -34.00 | 2.772 | 4.684 | 4.185 | 1.730 | 1.834 | 1.816 |
| 65 | -23.99 | -17.69 | -33.97 | 3.063 | 6.660 | 5.132 | 1.754 | 1.882 | 1.848 |
| 70 | -24.15 | -17.82 | -34.09 | 2.978 | 8.311 | 5.955 | 1.747 | 1.905 | 1.868 |
| 75 | -24.05 | -17.71 | -33.93 | 2.791 | 5.764 | 4.491 | 1.732 | 1.864 | 1.828 |
| 80 | -23.92 | -17.55 | -33.96 | 3.090 | 4.210 | 3.806 | 1.756 | 1.817 | 1.799 |
| 85 | -24.12 | -17.68 | -34.11 | 3.327 | 4.234 | 3.966 | 1.772 | 1.818 | 1.806 |
| 90 | -24.16 | -17.84 | -34.12 | 3.463 | 6.083 | 4.658 | 1.780 | 1.871 | 1.834 |
| 95 | -24.05 | -17.88 | -34.04 | 3.013 | 8.166 | 4.056 | 1.750 | 1.903 | 1.810 |
| 100 | -24.16 | -17.91 | -33.80 | 3.532 | 6.292 | 3.971 | 1.784 | 1.875 | 1.807 |
| 105 | -24.40 | -17.96 | -33.98 | 4.842 | 6.616 | 5.057 | 1.840 | 1.881 | 1.846 |
| 110 | -24.60 | -18.25 | -34.15 | 4.444 | 7.629 | 5.735 | 1.826 | 1.896 | 1.864 |
| 115 | -24.53 | -18.37 | -33.98 | 4.211 | 10.744 | 5.445 | 1.817 | 1.926 | 1.857 |
| 120 | -24.64 | -18.48 | -33.84 | 4.824 | 11.424 | 5.250 | 1.839 | 1.930 | 1.852 |
| 125 | -25.00 | -18.84 | -34.20 | 5.338 | 13.029 | 7.385 | 1.854 | 1.939 | 1.893 |
| 130 | -25.38 | -19.37 | -34.40 | 6.565 | 15.548 | 7.717 | 1.880 | 1.948 | 1.898 |
| 135 | -25.59 | -19.77 | -34.35 | 6.876 | 18.028 | 6.586 | 1.885 | 1.955 | 1.881 |
| 140 | -25.92 | -20.45 | -34.66 | 5.883 | 15.868 | 5.695 | 1.867 | 1.949 | 1.863 |
| 145 | -26.55 | -21.29 | -35.27 | 5.707 | 11.171 | 5.599 | 1.863 | 1.929 | 1.860 |
| 150 | -26.57 | -21.80 | -35.35 | 4.664 | 10.638 | 5.300 | 1.834 | 1.925 | 1.853 |
| 155 | -26.09 | -21.59 | -34.84 | 4.484 | 12.743 | 4.961 | 1.827 | 1.937 | 1.843 |
| 160 | -25.39 | -21.38 | -34.16 | 4.313 | 11.094 | 5.286 | 1.821 | 1.928 | 1.852 |
| 165 | -25.71 | -21.78 | -34.59 | 4.835 | 10.059 | 6.716 | 1.839 | 1.921 | 1.883 |
| 170 | -25.25 | -21.57 | -34.41 | 4.758 | 11.059 | 5.777 | 1.837 | 1.928 | 1.865 |
| 175 | -25.51 | -21.42 | -34.41 | 4.862 | 7.930 | 5.302 | 1.840 | 1.900 | 1.853 |
| 180 | -25.22 | -21.06 | -34.57 | 4.098 | 6.743 | 3.762 | 1.812 | 1.883 | 1.796 |
| 185 | -24.74 | -20.52 | -34.46 | 3.921 | 6.713 | 4.033 | 1.804 | 1.883 | 1.809 |
| 190 | -24.04 | -19.71 | -34.00 | 4.684 | 8.556 | 4.690 | 1.834 | 1.907 | 1.835 |
| 195 | -23.34 | -18.83 | -33.42 | 5.853 | 11.080 | 4.594 | 1.866 | 1.928 | 1.831 |
| 200 | -22.74 | -18.16 | -33.21 | 5.422 | 9.276 | 4.994 | 1.856 | 1.914 | 1.844 |
| 205 | -22.37 | -17.69 | -33.08 | 5.106 | 7.288 | 4.808 | 1.848 | 1.892 | 1.839 |
| 210 | -21.84 | -17.25 | -32.97 | 5.417 | 9.285 | 5.606 | 1.856 | 1.914 | 1.861 |
| 215 | -21.45 | -16.84 | -32.73 | 5.567 | 9.821 | 7.137 | 1.860 | 1.919 | 1.889 |
| 220 | -21.00 | -16.41 | -32.62 | 5.315 | 9.775 | 6.654 | 1.853 | 1.919 | 1.882 |

| Azimuth angle ($^o$) | Mean amplitude in dB | | | K shape parameter $\nu$ | | | Weibull shape parameter $b$ | | |
|---|---|---|---|---|---|---|---|---|---|
| | HH | VV | HV | HH | VV | HV | HH | VV | HV |
| 225 | -20.56 | -15.96 | -32.55 | 4.158 | 9.629 | 5.800 | 1.815 | 1.917 | 1.865 |
| 230 | -20.47 | -15.88 | -32.73 | 3.953 | 9.137 | 6.164 | 1.806 | 1.913 | 1.873 |
| 235 | -20.58 | -16.03 | -32.98 | 4.888 | 12.974 | 6.598 | 1.841 | 1.938 | 1.881 |
| 240 | -20.59 | -16.09 | -33.14 | 5.631 | 10.819 | 6.233 | 1.861 | 1.926 | 1.874 |
| 245 | -20.52 | -15.99 | -33.14 | 5.601 | 9.958 | 6.654 | 1.860 | 1.920 | 1.882 |
| 250 | -20.27 | -15.86 | -33.01 | 5.762 | 10.079 | 8.299 | 1.864 | 1.921 | 1.905 |
| 255 | -20.02 | -15.71 | -32.95 | 5.017 | 11.752 | 9.218 | 1.845 | 1.932 | 1.914 |
| 260 | -20.07 | -15.72 | -32.88 | 4.930 | 14.392 | 9.070 | 1.842 | 1.944 | 1.912 |
| 265 | -20.21 | -15.88 | -32.94 | 4.620 | 12.684 | 7.058 | 1.832 | 1.937 | 1.888 |
| 270 | -20.41 | -16.06 | -32.74 | 5.542 | 14.756 | 6.738 | 1.859 | 1.946 | 1.883 |
| 275 | -20.56 | -16.30 | -32.75 | 5.428 | 12.174 | 7.266 | 1.856 | 1.934 | 1.891 |
| 280 | -21.10 | -17.48 | -33.36 | 6.677 | 9.286 | 6.791 | 1.882 | 1.914 | 1.884 |
| 285 | -21.30 | -17.84 | -33.43 | 5.978 | 11.600 | 8.775 | 1.869 | 1.931 | 1.910 |
| 290 | -21.71 | -18.13 | -33.86 | 5.000 | 13.261 | 7.692 | 1.844 | 1.940 | 1.897 |
| 295 | -22.07 | -18.40 | -33.91 | 4.904 | 10.490 | 5.789 | 1.842 | 1.924 | 1.865 |
| 300 | -22.15 | -18.51 | -33.48 | 4.743 | 9.808 | 6.644 | 1.836 | 1.919 | 1.882 |
| 305 | -22.43 | -18.10 | -32.92 | 5.297 | 11.041 | 5.712 | 1.853 | 1.928 | 1.863 |
| 310 | -23.09 | -18.74 | -33.43 | 5.101 | 12.294 | 8.459 | 1.847 | 1.935 | 1.906 |
| 315 | -23.69 | -19.53 | -33.89 | 4.414 | 12.011 | 8.475 | 1.825 | 1.933 | 1.906 |
| 320 | -24.30 | -20.36 | -34.66 | 3.841 | 10.225 | 5.922 | 1.800 | 1.922 | 1.868 |
| 325 | -24.52 | -20.63 | -34.45 | 4.056 | 10.727 | 5.564 | 1.810 | 1.926 | 1.860 |
| 330 | -24.79 | -20.74 | -34.14 | 4.058 | 9.344 | 6.399 | 1.810 | 1.915 | 1.877 |
| 335 | -25.86 | -21.40 | -34.83 | 3.688 | 8.569 | 4.570 | 1.793 | 1.907 | 1.831 |

*Table A-2: Mean and shape parameters estimated for run34690 (incidence angle of 67.2°).*

| Azimuth | Mean amplitude in dB | | | K shape parameter $\nu$ | | | Weibull shape parameter $b$ | | |
|---|---|---|---|---|---|---|---|---|---|
| angle (°) | HH | VV | HV | HH | VV | HV | HH | VV | HV |
| 0 | -33.39 | -26.18 | -38.64 | 3.243 | 16.276 | 6.836 | 1.766 | 1.951 | 1.885 |
| 5 | -33.43 | -25.68 | -38.56 | 3.200 | 15.524 | 7.925 | 1.763 | 1.948 | 1.900 |
| 10 | -33.27 | -25.07 | -38.27 | 3.242 | 11.035 | 7.112 | 1.766 | 1.928 | 1.889 |
| 15 | -33.56 | -24.82 | -38.49 | 3.664 | 7.014 | 6.029 | 1.791 | 1.888 | 1.870 |
| 20 | -33.39 | -24.24 | -38.20 | 3.630 | 7.613 | 7.187 | 1.790 | 1.896 | 1.890 |
| 25 | -33.27 | -23.56 | -38.20 | 4.052 | 10.415 | 9.818 | 1.810 | 1.924 | 1.919 |
| 30 | -32.84 | -22.97 | -37.86 | 3.375 | 13.492 | 8.284 | 1.775 | 1.941 | 1.904 |
| 35 | -32.51 | -22.66 | -37.65 | 3.154 | 12.197 | 8.747 | 1.760 | 1.935 | 1.909 |
| 40 | -32.54 | -22.42 | -37.72 | 3.362 | 11.330 | 9.295 | 1.774 | 1.930 | 1.915 |
| 45 | -32.43 | -22.10 | -37.59 | 3.137 | 8.315 | 7.261 | 1.759 | 1.905 | 1.891 |
| 50 | -32.15 | -21.91 | -37.59 | 3.132 | 7.814 | 6.800 | 1.759 | 1.899 | 1.884 |
| 55 | -32.25 | -21.84 | -37.65 | 3.314 | 11.174 | 8.602 | 1.771 | 1.929 | 1.908 |
| 60 | -32.29 | -21.97 | -37.79 | 3.374 | 13.587 | 10.694 | 1.775 | 1.941 | 1.925 |
| 65 | -32.36 | -21.99 | -37.86 | 4.002 | 13.627 | 10.114 | 1.808 | 1.941 | 1.921 |
| 70 | -32.22 | -21.89 | -37.65 | 3.695 | 15.299 | 11.039 | 1.793 | 1.948 | 1.928 |
| 75 | -32.11 | -21.84 | -37.59 | 3.618 | 17.817 | 10.153 | 1.789 | 1.955 | 1.922 |
| 80 | -32.04 | -21.80 | -37.52 | 3.567 | 17.362 | 9.582 | 1.786 | 1.954 | 1.917 |
| 85 | -31.94 | -21.87 | -37.46 | 3.602 | 13.765 | 10.980 | 1.788 | 1.942 | 1.927 |
| 90 | -31.67 | -21.72 | -37.27 | 3.271 | 9.885 | 8.300 | 1.768 | 1.920 | 1.905 |
| 95 | -31.57 | -21.79 | -37.52 | 3.387 | 12.347 | 7.692 | 1.776 | 1.935 | 1.897 |
| 100 | -31.67 | -22.57 | -37.99 | 3.747 | 15.686 | 9.171 | 1.796 | 1.949 | 1.913 |
| 105 | -31.73 | -22.64 | -38.20 | 3.380 | 12.421 | 7.812 | 1.775 | 1.936 | 1.899 |
| 110 | -31.18 | -22.55 | -37.79 | 2.825 | 13.793 | 6.335 | 1.735 | 1.942 | 1.876 |
| 115 | -31.63 | -22.71 | -38.06 | 3.647 | 17.247 | 8.415 | 1.790 | 1.953 | 1.906 |
| 120 | -31.90 | -23.10 | -38.42 | 3.420 | 17.787 | 8.047 | 1.778 | 1.955 | 1.902 |
| 125 | -32.11 | -23.41 | -38.49 | 3.396 | 16.050 | 9.410 | 1.776 | 1.950 | 1.916 |
| 130 | -32.40 | -23.82 | -38.94 | 3.556 | 13.412 | 6.537 | 1.785 | 1.940 | 1.880 |
| 135 | -33.03 | -24.72 | -39.58 | 3.691 | 18.367 | 7.082 | 1.793 | 1.956 | 1.889 |
| 140 | -33.00 | -25.34 | -39.91 | 3.176 | 18.192 | 7.398 | 1.762 | 1.956 | 1.893 |
| 145 | -32.32 | -25.43 | -39.25 | 2.983 | 20.221 | 7.197 | 1.748 | 1.960 | 1.890 |
| 150 | -32.69 | -26.30 | -40.00 | 2.827 | 13.951 | 6.567 | 1.735 | 1.943 | 1.880 |
| 155 | -32.58 | -26.88 | -40.09 | 2.515 | 10.589 | 7.742 | 1.705 | 1.925 | 1.898 |
| 160 | -31.60 | -25.95 | -39.66 | 2.514 | 12.145 | 7.091 | 1.705 | 1.934 | 1.889 |
| 165 | -31.28 | -25.83 | -40.00 | 2.512 | 12.211 | 7.128 | 1.705 | 1.935 | 1.889 |
| 170 | -31.67 | -26.11 | -40.63 | 2.594 | 10.686 | 11.747 | 1.713 | 1.925 | 1.932 |
| 175 | -31.09 | -25.19 | -40.00 | 2.304 | 8.295 | 6.927 | 1.681 | 1.905 | 1.886 |
| 180 | -30.31 | -24.21 | -39.02 | 2.617 | 12.296 | 10.111 | 1.715 | 1.935 | 1.921 |
| 185 | -29.66 | -23.70 | -39.41 | 2.294 | 10.326 | 8.695 | 1.680 | 1.923 | 1.909 |
| 195 | -29.90 | -22.52 | -37.59 | 2.509 | 9.972 | 8.384 | 1.704 | 1.920 | 1.906 |
| 200 | -29.53 | -22.09 | -37.46 | 2.285 | 10.683 | 8.413 | 1.679 | 1.925 | 1.906 |
| 205 | -29.04 | -21.64 | -36.71 | 2.462 | 12.939 | 11.092 | 1.699 | 1.938 | 1.928 |
| 210 | -28.78 | -21.11 | -36.95 | 2.425 | 16.053 | 10.231 | 1.695 | 1.950 | 1.922 |
| 215 | -28.38 | -20.85 | -36.77 | 2.280 | 17.587 | 10.520 | 1.678 | 1.954 | 1.924 |
| 220 | -28.38 | -20.77 | -36.89 | 2.525 | 14.453 | 10.684 | 1.706 | 1.945 | 1.925 |
| 225 | -28.13 | -20.52 | -36.54 | 2.261 | 16.969 | 14.647 | 1.676 | 1.953 | 1.945 |
| 230 | -28.05 | -20.35 | -36.89 | 2.448 | 17.563 | 10.799 | 1.698 | 1.954 | 1.926 |
| 235 | -27.87 | -20.26 | -36.59 | 2.392 | 15.884 | 12.980 | 1.691 | 1.949 | 1.938 |
| 240 | -27.94 | -20.27 | -36.71 | 2.445 | 12.552 | 12.832 | 1.697 | 1.936 | 1.938 |
| 245 | -28.13 | -20.31 | -37.02 | 2.928 | 14.184 | 16.430 | 1.743 | 1.944 | 1.951 |
| 250 | -28.09 | -20.29 | -36.89 | 2.529 | 12.559 | 12.800 | 1.707 | 1.936 | 1.938 |

| Azimuth angle ($^o$) | Mean amplitude in dB | | | K shape parameter $\nu$ | | | Weibull shape parameter $b$ | | |
|---|---|---|---|---|---|---|---|---|---|
| | HH | VV | HV | HH | VV | HV | HH | VV | HV |
| 255 | -28.20 | -20.26 | -36.89 | 2.863 | 13.059 | 12.374 | 1.738 | 1.939 | 1.935 |
| 260 | -28.34 | -20.34 | -36.95 | 2.667 | 11.552 | 13.498 | 1.720 | 1.931 | 1.941 |
| 265 | -28.40 | -20.75 | -37.33 | 2.939 | 10.825 | 11.587 | 1.744 | 1.926 | 1.931 |
| 270 | -28.07 | -21.13 | -37.52 | 2.661 | 12.918 | 11.317 | 1.720 | 1.938 | 1.930 |
| 275 | -28.22 | -21.17 | -37.39 | 2.870 | 15.191 | 14.879 | 1.738 | 1.947 | 1.946 |
| 280 | -28.38 | -21.26 | -37.33 | 3.128 | 16.232 | 12.645 | 1.758 | 1.951 | 1.937 |
| 285 | -28.43 | -21.31 | -37.39 | 3.030 | 19.647 | 17.873 | 1.751 | 1.959 | 1.955 |
| 290 | -28.52 | -21.36 | -37.39 | 2.927 | 25.950 | 16.400 | 1.743 | 1.969 | 1.951 |
| 295 | -28.68 | -21.44 | -37.33 | 3.010 | 24.836 | 13.452 | 1.750 | 1.968 | 1.941 |
| 300 | -28.85 | -21.67 | -37.27 | 2.743 | 20.964 | 11.829 | 1.727 | 1.962 | 1.932 |
| 305 | -29.32 | -22.06 | -37.39 | 2.936 | 12.352 | 11.842 | 1.744 | 1.935 | 1.933 |
| 310 | -30.09 | -22.53 | -37.92 | 3.173 | 10.014 | 15.418 | 1.762 | 1.921 | 1.948 |
| 315 | -30.75 | -23.09 | -38.20 | 3.288 | 12.394 | 14.242 | 1.769 | 1.936 | 1.944 |
| 320 | -30.72 | -23.45 | -37.99 | 2.885 | 13.399 | 11.731 | 1.740 | 1.940 | 1.932 |
| 325 | -30.78 | -23.64 | -37.72 | 3.219 | 10.464 | 10.225 | 1.765 | 1.924 | 1.922 |
| 330 | -31.47 | -24.34 | -38.27 | 2.910 | 8.028 | 9.906 | 1.742 | 1.901 | 1.920 |
| 335 | -32.15 | -25.53 | -39.02 | 2.803 | 9.474 | 8.833 | 1.733 | 1.916 | 1.910 |
| 340 | -31.87 | -25.78 | -38.71 | 2.635 | 8.521 | 8.161 | 1.717 | 1.907 | 1.903 |
| 345 | -31.70 | -25.61 | -37.92 | 2.511 | 6.310 | 5.232 | 1.705 | 1.876 | 1.851 |
| 350 | -32.40 | -25.93 | -38.13 | 2.574 | 8.883 | 6.497 | 1.711 | 1.911 | 1.879 |
| 355 | -32.92 | -26.16 | -38.42 | 2.871 | 13.504 | 6.955 | 1.739 | 1.941 | 1.887 |

*Table A-3: Estimated KK and WW parameters for run34683 (incidence angle of 51.3°).*

| Azimuth angle (°) | KK parameters | | | | WW parameters | | | |
|---|---|---|---|---|---|---|---|---|
| | $k$ | $\rho$ (HH) | $\rho$ (VV) | $\rho$ (HV) | $k$ | $\rho$ (HH) | $\rho$ (VV) | $\rho$ (HV) |
| 0 | 0.01 | 3.38 | 1.20 | 3.71 | 0.01 | 4.06 | 2.59 | 4.22 |
| 5 | 0.01 | 3.28 | 1.00 | 3.25 | 0.01 | 4.03 | 2.16 | 3.89 |
| 10 | 0.01 | 4.13 | 1.04 | 3.71 | 0.01 | 4.97 | 2.29 | 4.29 |
| 15 | 0.01 | 4.76 | 1.00 | 5.30 | 0.01 | 5.69 | 2.13 | 5.93 |
| 20 | 0.01 | 4.65 | 1.00 | 4.52 | 0.01 | 5.40 | 1.91 | 4.92 |
| 25 | 0.01 | 4.04 | 1.00 | 3.94 | 0.01 | 4.71 | 2.12 | 4.47 |
| 30 | 0.01 | 4.14 | 1.00 | 3.40 | 0.01 | 5.01 | 2.55 | 4.30 |
| 35 | 0.01 | 3.55 | 1.00 | 3.44 | 0.01 | 4.68 | 2.54 | 4.45 |
| 40 | 0.01 | 3.70 | 1.00 | 3.63 | 0.01 | 4.72 | 2.39 | 4.46 |
| 45 | 0.01 | 3.51 | 1.66 | 3.18 | 0.01 | 4.54 | 2.96 | 4.06 |
| 50 | 0.01 | 3.55 | 2.17 | 3.84 | 0.01 | 4.59 | 3.37 | 4.57 |
| 55 | 0.01 | 4.42 | 2.74 | 4.97 | 0.01 | 5.55 | 3.83 | 5.88 |
| 60 | 0.01 | 3.70 | 2.35 | 4.17 | 0.01 | 4.81 | 3.52 | 5.04 |
| 65 | 0.01 | 2.37 | 1.00 | 3.04 | 0.01 | 3.74 | 2.55 | 3.90 |
| 70 | 0.01 | 3.05 | 1.00 | 3.76 | 0.01 | 4.19 | 2.60 | 4.49 |
| 75 | 0.01 | 3.67 | 1.97 | 4.01 | 0.01 | 4.81 | 3.21 | 4.76 |
| 80 | 0.01 | 4.02 | 1.00 | 3.02 | 0.01 | 5.30 | 2.88 | 4.04 |
| 85 | 0.01 | 2.45 | 1.00 | 3.03 | 0.01 | 3.77 | 2.71 | 4.05 |
| 90 | 0.01 | 2.69 | 1.00 | 3.21 | 0.01 | 3.89 | 2.50 | 4.12 |
| 95 | 0.01 | 4.97 | 1.74 | 5.93 | 0.01 | 6.11 | 2.89 | 6.88 |
| 100 | 0.01 | 3.25 | 2.09 | 3.50 | 0.01 | 4.21 | 3.12 | 4.38 |
| 105 | 0.01 | 3.02 | 1.00 | 3.16 | 0.01 | 3.89 | 2.76 | 3.99 |
| 110 | 0.01 | 3.91 | 1.00 | 3.39 | 0.01 | 4.73 | 2.70 | 4.12 |
| 115 | 0.01 | 3.35 | 1.16 | 3.37 | 0.01 | 4.35 | 2.43 | 4.22 |
| 120 | 0.01 | 2.75 | 1.00 | 2.82 | 0.01 | 3.79 | 2.18 | 3.71 |
| 125 | 0.01 | 3.33 | 1.34 | 3.81 | 0.01 | 4.10 | 2.46 | 4.28 |
| 130 | 0.01 | 3.60 | 1.00 | 4.31 | 0.01 | 4.30 | 2.10 | 4.78 |
| 135 | 0.01 | 2.59 | 1.00 | 2.47 | 0.01 | 3.44 | 1.84 | 3.40 |
| 140 | 0.01 | 4.51 | 1.00 | 2.56 | 0.01 | 5.16 | 2.04 | 3.56 |
| 145 | 0.01 | 4.02 | 1.00 | 2.78 | 0.01 | 4.83 | 2.17 | 3.69 |
| 150 | 0.01 | 4.03 | 1.65 | 3.82 | 0.01 | 4.85 | 2.69 | 4.48 |
| 155 | 0.01 | 4.44 | 1.38 | 4.48 | 0.01 | 5.20 | 2.45 | 5.23 |
| 160 | 0.01 | 4.16 | 1.70 | 3.11 | 0.01 | 4.95 | 2.57 | 3.92 |
| 165 | 0.01 | 2.78 | 1.00 | 2.64 | 0.01 | 3.70 | 2.27 | 3.47 |
| 170 | 0.01 | 3.96 | 1.42 | 3.17 | 0.01 | 4.68 | 2.58 | 3.92 |
| 175 | 0.01 | 3.99 | 1.50 | 3.21 | 0.01 | 4.73 | 2.82 | 4.03 |
| 180 | 0.01 | 3.50 | 1.07 | 3.05 | 0.01 | 4.39 | 2.84 | 4.06 |
| 185 | 0.01 | 3.96 | 1.26 | 2.95 | 0.01 | 4.88 | 2.87 | 3.96 |
| 190 | 0.01 | 5.77 | 2.69 | 2.07 | 0.01 | 6.88 | 3.50 | 3.43 |
| 195 | 0.01 | 3.28 | 1.31 | 1.86 | 0.01 | 4.01 | 2.39 | 3.31 |
| 200 | 0.01 | 3.57 | 1.00 | 1.52 | 0.01 | 4.33 | 2.37 | 3.14 |
| 205 | 0.01 | 3.00 | 1.00 | 1.75 | 0.01 | 3.97 | 2.61 | 3.22 |
| 210 | 0.01 | 2.88 | 1.16 | 1.84 | 0.01 | 3.79 | 2.53 | 3.13 |
| 215 | 0.01 | 4.69 | 1.46 | 1.07 | 0.01 | 5.60 | 2.55 | 2.69 |
| 220 | 0.01 | 3.15 | 1.00 | 1.00 | 0.01 | 4.13 | 2.24 | 2.68 |

| Azimuth angle ($^o$) | KK parameters | | | | WW parameters | | | |
|---|---|---|---|---|---|---|---|---|
| | $k$ | $\rho$ (HH) | $\rho$ (VV) | $\rho$ (HV) | $k$ | $\rho$ (HH) | $\rho$ (VV) | $\rho$ (HV) |
| 225 | 0.01 | 3.27 | 1.00 | 1.60 | 0.01 | 4.22 | 2.39 | 3.05 |
| 230 | 0.01 | 2.87 | 1.00 | 2.00 | 0.01 | 3.90 | 2.34 | 3.15 |
| 235 | 0.01 | 3.18 | 1.00 | 3.29 | 0.01 | 4.10 | 2.21 | 4.12 |
| 240 | 0.01 | 2.86 | 1.00 | 1.72 | 0.01 | 3.71 | 2.14 | 2.94 |
| 245 | 0.01 | 3.04 | 1.00 | 1.36 | 0.01 | 3.92 | 2.10 | 2.91 |
| 250 | 0.01 | 3.03 | 1.00 | 1.00 | 0.01 | 3.86 | 2.11 | 2.46 |
| 255 | 0.01 | 3.69 | 1.00 | 1.51 | 0.01 | 4.43 | 2.25 | 2.69 |
| 260 | 0.01 | 3.27 | 1.36 | 2.80 | 0.01 | 4.15 | 2.30 | 3.45 |
| 265 | 0.01 | 3.11 | 1.03 | 1.83 | 0.01 | 4.03 | 2.22 | 3.04 |
| 270 | 0.01 | 2.60 | 1.07 | 2.77 | 0.01 | 3.57 | 2.04 | 3.59 |
| 275 | 0.01 | 3.66 | 1.21 | 2.91 | 0.01 | 4.50 | 2.26 | 3.59 |
| 280 | 0.01 | 3.43 | 1.00 | 1.91 | 0.01 | 4.07 | 2.45 | 3.10 |
| 285 | 0.01 | 3.83 | 1.00 | 1.53 | 0.01 | 4.50 | 2.22 | 2.81 |
| 290 | 0.01 | 4.56 | 1.13 | 2.89 | 0.01 | 5.36 | 2.28 | 3.51 |
| 295 | 0.01 | 3.89 | 1.06 | 3.05 | 0.01 | 4.73 | 2.43 | 3.89 |
| 300 | 0.01 | 3.57 | 2.12 | 3.42 | 0.01 | 4.37 | 2.97 | 4.09 |
| 305 | 0.01 | 2.96 | 1.00 | 3.12 | 0.01 | 3.83 | 2.29 | 3.94 |
| 310 | 0.01 | 3.37 | 1.13 | 2.38 | 0.01 | 4.15 | 2.30 | 3.17 |
| 315 | 0.01 | 3.87 | 1.01 | 2.60 | 0.01 | 4.73 | 2.34 | 3.31 |
| 320 | 0.01 | 3.76 | 1.57 | 3.20 | 0.01 | 4.65 | 2.68 | 3.94 |
| 325 | 0.01 | 4.24 | 1.02 | 3.52 | 0.01 | 5.24 | 2.43 | 4.23 |
| 330 | 0.01 | 3.65 | 1.00 | 2.16 | 0.01 | 4.63 | 2.29 | 3.21 |
| 335 | 0.01 | 3.49 | 1.00 | 3.99 | 0.01 | 4.44 | 2.42 | 4.81 |
| 340 | 0.01 | 4.16 | 1.87 | 3.39 | 0.01 | 5.01 | 2.95 | 4.11 |
| 345 | 0.01 | 4.25 | 1.94 | 3.16 | 0.01 | 5.05 | 2.86 | 3.98 |
| 350 | 0.01 | 3.89 | 1.10 | 2.79 | 0.01 | 4.64 | 2.29 | 3.70 |
| 355 | 0.01 | 3.70 | 1.00 | 3.96 | 0.01 | 4.42 | 2.43 | 4.41 |

*Table A-4: Estimated KK and WW parameters for run34690 (incidence angle of 67.2°).*

| Azimuth angle (°) | KK parameters | | | | WW parameters | | | |
|---|---|---|---|---|---|---|---|---|
| | $k$ | $\rho$ (HH) | $\rho$ (VV) | $\rho$ (HV) | $k$ | $\rho$ (HH) | $\rho$ (VV) | $\rho$ (HV) |
| 0 | 0.01 | 5.19 | 1.37 | 3.40 | 0.01 | 6.16 | 2.59 | 4.01 |
| 5 | 0.01 | 6.22 | 1.85 | 4.44 | 0.01 | 7.37 | 2.16 | 4.93 |
| 10 | 0.01 | 8.78 | 1.07 | 5.93 | 0.01 | 10.67 | 2.29 | 6.71 |
| 15 | 0.01 | 5.74 | 1.00 | 3.04 | 0.01 | 6.71 | 2.13 | 3.84 |
| 20 | 0.01 | 6.62 | 1.00 | 3.31 | 0.01 | 7.85 | 1.91 | 3.94 |
| 25 | 0.01 | 5.75 | 1.00 | 2.99 | 0.01 | 6.64 | 2.12 | 3.50 |
| 30 | 0.01 | 7.44 | 1.00 | 3.86 | 0.01 | 8.78 | 2.55 | 4.37 |
| 35 | 0.01 | 7.41 | 1.00 | 3.33 | 0.01 | 8.76 | 2.54 | 3.82 |
| 40 | 0.01 | 6.46 | 1.00 | 3.08 | 0.01 | 7.63 | 2.39 | 3.64 |
| 45 | 0.01 | 6.36 | 1.06 | 3.57 | 0.01 | 7.54 | 2.96 | 4.14 |
| 50 | 0.01 | 5.11 | 1.00 | 2.37 | 0.01 | 6.24 | 3.37 | 3.30 |
| 55 | 0.01 | 5.45 | 1.00 | 3.32 | 0.01 | 6.43 | 3.83 | 3.85 |
| 60 | 0.01 | 6.29 | 1.00 | 3.17 | 0.01 | 7.44 | 3.52 | 3.62 |
| 65 | 0.01 | 4.78 | 1.00 | 3.03 | 0.01 | 5.63 | 2.55 | 3.49 |
| 70 | 0.01 | 5.16 | 1.00 | 2.73 | 0.01 | 6.03 | 2.60 | 3.23 |
| 75 | 0.01 | 5.26 | 1.00 | 2.98 | 0.01 | 6.21 | 3.21 | 3.46 |
| 80 | 0.01 | 6.12 | 1.00 | 3.25 | 0.01 | 7.21 | 2.88 | 3.71 |
| 85 | 0.01 | 7.28 | 1.00 | 3.48 | 0.01 | 8.52 | 2.71 | 3.82 |
| 90 | 0.01 | 5.40 | 1.15 | 3.29 | 0.01 | 6.48 | 2.50 | 3.80 |
| 95 | 0.01 | 6.15 | 1.17 | 4.33 | 0.01 | 7.19 | 2.89 | 4.79 |
| 100 | 0.01 | 6.77 | 1.00 | 3.78 | 0.01 | 7.92 | 3.12 | 4.14 |
| 105 | 0.01 | 6.99 | 1.00 | 4.72 | 0.01 | 8.22 | 2.76 | 5.12 |
| 110 | 0.01 | 8.46 | 1.06 | 5.76 | 0.01 | 10.03 | 2.70 | 6.31 |
| 115 | 0.01 | 6.03 | 1.00 | 3.48 | 0.01 | 7.13 | 2.43 | 3.95 |
| 120 | 0.01 | 9.11 | 1.00 | 4.88 | 0.01 | 10.87 | 2.18 | 5.31 |
| 125 | 0.01 | 6.74 | 1.00 | 3.99 | 0.01 | 7.95 | 2.46 | 4.34 |
| 130 | 0.01 | 7.05 | 1.00 | 4.87 | 0.01 | 8.21 | 2.10 | 5.45 |
| 135 | 0.01 | 5.88 | 1.00 | 3.68 | 0.01 | 6.85 | 1.84 | 4.20 |
| 140 | 0.01 | 6.99 | 1.43 | 4.63 | 0.01 | 8.27 | 2.04 | 5.03 |
| 145 | 0.01 | 6.08 | 1.57 | 3.69 | 0.01 | 7.38 | 2.17 | 4.23 |
| 150 | 0.01 | 6.65 | 1.00 | 3.02 | 0.01 | 8.09 | 2.69 | 3.71 |
| 155 | 0.01 | 7.35 | 1.88 | 4.39 | 0.01 | 8.90 | 2.45 | 4.89 |
| 160 | 0.01 | 5.75 | 1.49 | 2.76 | 0.01 | 7.02 | 2.57 | 3.46 |
| 165 | 0.01 | 6.49 | 2.02 | 3.19 | 0.01 | 7.86 | 2.27 | 3.84 |
| 170 | 0.01 | 9.23 | 3.67 | 3.19 | 0.01 | 11.11 | 2.58 | 3.61 |
| 175 | 0.01 | 6.64 | 1.39 | 3.40 | 0.01 | 8.09 | 2.82 | 4.03 |
| 180 | 0.01 | 6.51 | 1.00 | 3.39 | 0.01 | 7.87 | 2.84 | 3.88 |
| 185 | 0.01 | 8.67 | 1.69 | 5.76 | 0.01 | 10.53 | 2.87 | 6.18 |
| 195 | 0.01 | 6.98 | 1.00 | 1.26 | 0.01 | 8.55 | 3.50 | 2.62 |
| 200 | 0.01 | 7.82 | 1.25 | 1.26 | 0.01 | 9.51 | 2.39 | 2.60 |
| 205 | 0.01 | 6.39 | 1.09 | 1.85 | 0.01 | 7.77 | 2.37 | 2.80 |
| 210 | 0.01 | 7.13 | 1.10 | 1.94 | 0.01 | 8.58 | 2.61 | 2.87 |
| 215 | 0.01 | 7.10 | 1.00 | 2.30 | 0.01 | 8.67 | 2.53 | 3.17 |
| 220 | 0.01 | 6.08 | 1.15 | 2.37 | 0.01 | 7.39 | 2.55 | 3.24 |
| 225 | 0.01 | 7.34 | 1.71 | 3.25 | 0.01 | 8.91 | 2.24 | 3.60 |

| Azimuth angle ($^o$) | KK parameters | | | | WW parameters | | | |
|---|---|---|---|---|---|---|---|---|
| | $k$ | $\rho$ (HH) | $\rho$ (VV) | $\rho$ (HV) | $k$ | $\rho$ (HH) | $\rho$ (VV) | $\rho$ (HV) |
| 230 | 0.01 | 7.30 | 1.02 | 3.86 | 0.01 | 8.93 | 2.39 | 4.54 |
| 235 | 0.01 | 7.27 | 1.33 | 2.02 | 0.01 | 9.00 | 2.34 | 2.78 |
| 240 | 0.01 | 8.06 | 1.39 | 2.53 | 0.01 | 9.92 | 2.21 | 3.25 |
| 245 | 0.01 | 6.84 | 1.00 | 2.74 | 0.01 | 8.26 | 2.14 | 3.33 |
| 250 | 0.01 | 7.73 | 1.00 | 2.71 | 0.01 | 9.38 | 2.10 | 3.39 |
| 255 | 0.01 | 4.82 | 1.00 | 1.00 | 0.01 | 5.94 | 2.11 | 2.24 |
| 260 | 0.01 | 7.33 | 1.00 | 1.39 | 0.01 | 9.01 | 2.25 | 2.40 |
| 265 | 0.01 | 5.19 | 1.00 | 1.64 | 0.01 | 6.28 | 2.30 | 2.57 |
| 270 | 0.01 | 8.28 | 1.28 | 3.30 | 0.01 | 10.09 | 2.22 | 4.07 |
| 275 | 0.01 | 6.18 | 1.00 | 1.00 | 0.01 | 7.51 | 2.04 | 2.24 |
| 280 | 0.01 | 4.62 | 1.00 | 1.46 | 0.01 | 5.60 | 2.26 | 2.50 |
| 285 | 0.01 | 6.03 | 1.00 | 1.56 | 0.01 | 7.20 | 2.45 | 2.32 |
| 290 | 0.01 | 6.30 | 1.00 | 1.83 | 0.01 | 7.55 | 2.22 | 2.55 |
| 295 | 0.01 | 6.00 | 1.17 | 2.18 | 0.01 | 7.22 | 2.28 | 2.87 |
| 300 | 0.01 | 5.63 | 1.00 | 2.53 | 0.01 | 6.84 | 2.43 | 3.12 |
| 305 | 0.01 | 5.25 | 1.00 | 2.42 | 0.01 | 6.38 | 2.97 | 3.02 |
| 310 | 0.01 | 5.91 | 1.00 | 2.26 | 0.01 | 7.18 | 2.29 | 2.79 |
| 315 | 0.01 | 5.29 | 1.00 | 2.97 | 0.01 | 6.27 | 2.30 | 3.29 |
| 320 | 0.01 | 5.77 | 1.00 | 2.92 | 0.01 | 6.93 | 2.34 | 3.33 |
| 325 | 0.01 | 4.30 | 1.00 | 2.39 | 0.01 | 5.33 | 2.68 | 3.06 |
| 330 | 0.01 | 5.59 | 1.00 | 3.75 | 0.01 | 6.74 | 2.43 | 4.19 |
| 335 | 0.01 | 7.26 | 1.49 | 3.65 | 0.01 | 8.80 | 2.29 | 4.06 |
| 340 | 0.01 | 7.51 | 1.00 | 3.79 | 0.01 | 9.06 | 2.42 | 4.20 |
| 345 | 0.01 | 6.65 | 1.71 | 4.28 | 0.01 | 8.13 | 2.95 | 5.01 |
| 350 | 0.01 | 8.44 | 1.39 | 4.21 | 0.01 | 10.30 | 2.86 | 4.76 |
| 355 | 0.01 | 7.28 | 1.60 | 4.78 | 0.01 | 8.89 | 2.29 | 5.38 |

Distribution of X-Band High Resolution and High Grazing Angle Sea Clutter

Yunhan Dong

(DSTO-RR-0316)

**AUSTRALIA**

| **DEFENCE ORGANISATION** | **No. of copies** |
|---|---|
| **Task Sponsor:** DGAD | 1 printed |
| **S&T Program** | |
| Chief Defence Scientist | 1 |
| Deputy Chief Defence Scientist Policy | 1 |
| AS Science Corporate Management | 1 |
| Director General Science Policy Development | 1 |
| Counsellor Defence Science, London | Doc Data Sheet |
| Counsellor Defence Science, Washington | Doc Data Sheet |
| Scientific Adviser to MRDC, Thailand | Doc Data Sheet |
| Scientific Adviser Joint | 1 |
| Navy Scientific Adviser | 1 |
| Scientific Adviser – Army | 1 |
| AirForce Scientific Adviser | 1 |
| Scientific Adviser to the DMO | 1 |
| Deputy Chief Defence Scientist Platform and Human Systems | Doc Data Sht & Exec Summ |
| EWSTIS (soft copy for accession to EWSTIS Web site) | 1 |
| Chief, Electronic Warfare and Radar Division | Doc Data Sht & Dist List |
| Head, Maritime Air Surface | 1 |
| Peter Khan Sharp (Director of Air7000) | 1 |
| Rodney Smith (ISRD) | 1 |
| Warren McDonald (MUAS AIR700 IPT SQNLDR) | 1 |
| Kevin Murray (MPR AIR7000IPT SQNLDR) | 1 |
| David Cox (AOD) | 1 |
| David Crisp (ISRD) | 1 printed |
| Yunhan Dong, EWRD | 1 printed |
| **DSTO Library and Archives** | |
| Library Edinburgh | 1 printed |
| Defence Archives | 1 printed |
| **Capability Development Group** | |
| Director General Maritime Development | Doc Data Sheet |
| Director General Capability and Plans | Doc Data Sheet |
| Assistant Secretary Investment Analysis | Doc Data Sheet |
| Director Capability Plans and Programming | Doc Data Sheet |

| | |
|---|---|
| **Chief Information Officer Group** | |
| Director General Australian Defence Simulation Office | Doc Data Sheet |
| AS Information Strategy and Futures | Doc Data Sheet |
| Director General Information Services | Doc Data Sheet |
| **Strategy Group** | |
| Assistant Secretary Strategic Planning | Doc Data Sheet |
| Assistant Secretary Governance and Counter-Proliferation | Doc Data Sheet |
| **Navy** | |
| **Maritime Operational Analysis Centre, Building 89/90 Garden Island Sydney NSW** | Doc Data Sht & Dist List |
| Deputy Director (Operations) | |
| Deputy Director (Analysis) | |
| Director General Navy Capability, Performance and Plans, Navy Headquarters | Doc Data Sheet |
| Director General Navy Strategic Policy and Futures, Navy Headquarters | Doc Data Sheet |
| **Air Force** | |
| SO (Science) - Headquarters Air Combat Group, RAAF Base, Williamtown NSW 2314 | Doc Data Sht & Exec Summ |
| **Army** | |
| **ABCA National Standardisation Officer** | e-mailed Doc Data Sheet |
| Land Warfare Development Sector, Puckapunyal | |
| J86 (TCS GROUP), DJFHQ | Doc Data Sht |
| SO (Science) - Land Headquarters (LHQ), Victoria Barracks NSW | Doc Data Sht & Exec Summ |
| SO (Science), Deployable Joint Force Headquarters (DJFHQ) (L), Enoggera QLD | Doc Data Sheet |
| **Joint Operations Command** | |
| Director General Joint Operations | Doc Data Sheet |
| Chief of Staff Headquarters Joint Operations Command | Doc Data Sheet |
| Commandant ADF Warfare Centre | Doc Data Sheet |
| Director General Strategic Logistics | Doc Data Sheet |
| COS Australian Defence College | Doc Data Sheet |
| **Intelligence and Security Group** | |
| AS Concepts, Capability and Resources | 1 |
| DGSTA , DIO | 1 |
| Manager, Information Centre, Defence Intelligence Organisation | 1 |
| Director Advanced Capabilities | Doc Data Sheet |
| **Defence Materiel Organisation** | |
| Deputy CEO | Doc Data Sheet |

| | |
|---|---|
| Head Aerospace Systems Division | Doc Data Sheet |
| Head Maritime Systems Division | Doc Data Sheet |
| Program Manager Air Warfare Destroyer | Doc Data Sheet |
| Guided Weapon & Explosive Ordnance Branch (GWEO) | Doc Data Sheet |
| CDR Joint Logistics Command | Doc Data Sheet |

**OTHER ORGANISATIONS**

| | |
|---|---|
| National Library of Australia | 1 |
| NASA (Canberra) | 1 |

**UNIVERSITIES AND COLLEGES**

| | |
|---|---|
| Australian Defence Force Academy | |
| Library | 1 |
| Head of Aerospace and Mechanical Engineering | 1 |
| Hargrave Library, Monash University | Doc Data Sheet |

**OUTSIDE AUSTRALIA**

**INTERNATIONAL DEFENCE INFORMATION CENTRES**

| | |
|---|---|
| US Defense Technical Information Center | 1 |
| UK Dstl Knowledge Services | 1 |
| Canada Defence Research Directorate R&D Knowledge & Information Management (DRDKIM) | 1 |
| NZ Defence Information Centre | 1 |

**ABSTRACTING AND INFORMATION ORGANISATIONS**

| | |
|---|---|
| Library, Chemical Abstracts Reference Service | 1 |
| Engineering Societies Library, US | 1 |
| Materials Information, Cambridge Scientific Abstracts, US | 1 |
| Documents Librarian, The Center for Research Libraries, US | 1 |

**INFORMATION EXCHANGE AGREEMENT PARTNERS**

| | |
|---|---|
| National Aerospace Laboratory, Japan | 1 |
| National Aerospace Laboratory, Netherlands | 1 |

| | |
|---|---|
| SPARES | 5 printed |

**Total number of copies: 43 Printed: 10 PDF: 33**

Page classification: UNCLASSIFIED

**DEFENCE SCIENCE AND TECHNOLOGY ORGANISATION**
**DOCUMENT CONTROL DATA**

1. PRIVACY MARKING/CAVEAT (OF DOCUMENT)

2. TITLE

Distribution of X-Band High Resolution and High Grazing Angle Sea Clutter

3. SECURITY CLASSIFICATION (FOR UNCLASSIFIED REPORTS THAT ARE LIMITED RELEASE USE (L) NEXT TO DOCUMENT CLASSIFICATION)

Document (U)
Title (U)
Abstract (U)

4. AUTHOR(S)

Yunhan Dong

5. CORPORATE AUTHOR

Defence Science and Technology Organisation
PO Box 1500
Edinburgh SA 5111

| 6a. DSTO NUMBER | 6b. AR NUMBER | 6c. TYPE OF REPORT | 7. DOCUMENT DATE |
|---|---|---|---|
| DSTO-RR-0316 | AR-013-708 | Research Report | July 2006 |

| 8. FILE NUMBER | 9. TASK NUMBER | 10. TASK SPONSOR | 11. NO. OF PAGES | 12. NO. OF REFERENCES |
|---|---|---|---|---|
| 20005/1062004 | AIR 05/263 | DGAD | 88 | 31 |

13. URL on the World Wide Web
http://www.dsto.defence.gov.au/corporate/reports/DSTO-RR-0316.pdf

14. RELEASE AUTHORITY

Chief, Electronic Warfare and Radar Division

15. SECONDARY RELEASE STATEMENT OF THIS DOCUMENT

Approved for Public Release

OVERSEAS ENQUIRIES OUTSIDE STATED LIMITATIONS SHOULD BE REFERRED TO DOCUMENT EXCHANGE, PO BOX 1500, EDINBURGH, SA 5111, AUSTRALIA

16. DELIBERATE ANNOUNCEMENT

No Limitations

17. CASUAL ANNOUNCEMENT Yes

18. DSTO RESEARCH LIBRARY THESAURUS

Sea clutter
Azimuth
Incidence angle
Ingara

19. ABSTRACT

This report studies the spatial distribution of X-band, high resolution and high grazing angle polarimetric sea clutter data. The K distribution usually provides a good fit for the distribution of the VV polarised data. The HH polarised data is spikiest and its distribution exhibits a sudden departure from the K distribution in the tail region, which usually requires the KA or the similar distributions to achieve a better fit in the tail region. Due to drawbacks of the KA distribution, this report proposes the KK and WW distribution models to fit the distribution of sea clutter with spikes. It is found that the KK distribution provides overall the best fit. Distributions of the sum of K and Weibull distributed samples are also presented.